arXiv:2206.03120v1 [nlin.CD] 7 Jun 2022

Topical Review
Spatio-temporal phenomena in complex systems with time delays

Serhiy Yanchuk[1] and Giovanni Giacomelli[2]

June 10, 2022

[1]Technische Universität Berlin, Institute of Mathematics, Straße des 17. Juni 136, 10623 Berlin, Germany

[2]CNR-Istituto dei Sistemi Complessi, via Madonna del Piano 10, I-50019 Sesto Fiorentino (FI), Italy

Contents

Abstract

Real-world systems can be strongly influenced by time delays occurring in self-coupling interactions, due to the unavoidable finite signal propagation velocities. When the delays become significantly long, complicated high-dimensional phenomena appear and a simple extension of the methods employed in low-dimensional dynamical systems is not feasible. We review the general theory developed in this case, describing the main destabilization mechanisms, the use of visualization tools and commenting the most important and effective dynamical indicators and their properties in different regimes. We show how a suitable approach, based on the comparison with spatio-temporal system represents a powerful instrument to disclose the very basic mechanism of long delay systems. Various examples from different models and a series of recent experiments are reported.

1 Introduction

The utmost important missions of nonlinear dynamics are certainly the understanding of the working principles of complex real-world or artificial systems, and predicting and controlling their behaviors. Several dynamical systems have proven their surprising effectiveness in modeling specific experiments and natural phenomena; the most common belong to the class of ordinary differential systems (ODS), discrete-time systems, or partial differential equations. While the first two are finite-dimensional and determine the dynamics on the basis of finitely many variables, the latter is infinite-dimensional, and it is commonly employed to describe the evolution of spatially-extended systems

Another extremely useful mathematical tool is represented by delay-differential systems (DDS), which play a special role within the toolbox of dynamical systems. Starting from the sixties of the last century up to now, the use of such systems spread into practically all possible application fields, ranging from biology and neuroscience [1, 2, 3], laser physics [4, 5, 6, 7], to population dynamics[8], quantum physics [9], and traffic systems [10] just to name a few. In contrast to finite-dimensional systems, DDS take into account the time lags, which appear naturally in realistic models when properly keeping in account the finite propagation times of the signals, finite reaction times or velocity of bodies. An exemplary situation is represented by the retarded potentials in classical electrodynamics [11, 12]; their effect can also lead to some surprising consequences [13].

In 1977, Mackey and Glass introduced a simple-looking, scalar physiological control system with time delay showing surprisingly rich dynamical behaviors including deterministic chaos [1]. Two years later Ikeda proposed a delay model for the ring laser [4], which was very popular till nowadays. Apart from their elegance and apparent simplicity, the success and importance of these models was incepted by a proper timing. At that time, research on deterministic chaos was rising, and the above mentioned models were among the utmost examples of simple-at-a-glance, time-continuous scalar systems exhibiting chaotic dynamics. A further, very important model was suggested by Lang and Kobayashi [14] in 1980 for a semiconductor laser with delayed feedback, and it appeared to be extremely useful in describing the dynamics even on a quantitative level in some situations.

In all the aforementioned systems, the time delay is a parameter of paramount importance. The early study of the qualitative properties of chaotic attractors in DDS, and especially their dependence on time delay, was carried out by Farmer in [15]. The mathematical analysis of DDS can be dated back at least to 1949 [16], since then, it has been developed significantly [17, 18, 19, 20, 21, 22]. Early mathematical results on systems with possibly large time delays, relevant for the purpose of this review include the contributions of Mallet-Paret and Nussbaum on systems with monotone delayed feedback [23, 24], in particular, the appearance of square waves. Kashchenko et al. [25, 26, 27, 28, 29] reported about the formal asymptotic reductions of multiscale delay systems to partial differential equations.

The simplest DDS with a single time delay τ has the form

$$\frac{dx}{dt}(t) = F(x(t), x(t-\tau)), \tag{1}$$

similar to a system of ordinary differential equations[1]; however, the presence of the time delay implies that its phase space is infinite-dimensional. Indeed, this fact was pointed out already by the very first researches [30]. In particular, an initial condition for this system should be given as a function on the interval of length τ, i.e. $x_0(\theta)$, $\theta \in [-\tau, 0]$, if evolution $x(t)$ is to be found for $t > 0$. Such segments of function of length τ can be considered as points in the infinite-dimensional phase space, and the system (1) describes the evolution in such a phase space. Accordingly, the notation x_t is sometimes used in the mathematical literature to denote such a "point" at time t: $x_t := x_t(\theta)$, $\theta \in [-\tau, 0]$.

DDS are infinite-dimensional even for very small delay. This statement would seemingly lead us to a contradiction with a common sense that very small time delays should not make any effect on the dynamics, and, thus, the system in such a case should be finite dimensional. This contradiction is resolved by the fact that DDS, being formally infinite dimensional systems, exhibit a dynamics which is essentially *finitely* dimensional. Using a more precise mathematical language, this means that the system's dynamics $x(t)$ approaches a certain finite-dimensional attractor or manifold. For small time delays $\tau \to 0$, this can also be shown rigorously [31]. In such a case, the dynamics on the manifold is governed by the reduced finite-dimensional system $x' = F(x, x)$. As the time delay increases, the complexity often increases as well as the dimensionality of the dynamics [15, 32, 33, 34, 35, 36, 37, 38, 39, 40, 41, 42] leading to new phenomena and increased coexistence of different attractors. Meanwhile, it is commonly accepted that the effective dimensionality of the systems can become arbitrary large as the delay grows [43, 38, 44, 45, 46, 47, 48, 49].

The following points stay at the very basis of the message of this review:

1. Time delay systems can exhibit dynamical phenomena that can be arbitrary high-dimensional. A more precise meaning of this will be made clear in the subsequent sections of the article.

2. The dimensionality of the observed phenomena is proportional to the time delay τ.

3. A proper description of the high-dimensional dynamics in DDSs requires methods, that are different from those used for low-dimensional ODE systems. In particular, the normal forms that describe the destabilization processes are sometimes similar to those for spatially extended systems (PDEs).

Along the review, we will try to clarify the above general statements and make them more precise, as well as to present a variety of realizations of the spectacular high-dimensional phenomena exhibited by DDS, their theoretical analysis and experimental applications.

In order to make this paper more focused, we decided not to treat the role of noise on the dynamics. It is widely considered in the literature (see e.g. the special issue [50]) and it would deserve a separate detailed discussion.

[1] Here we do not consider the situation when the derivative in (1) is delayed. Such systems are called neutral and possess several properties that differ them from (1), see [19].

The structure of this manuscript is the following. In Sec. 2, we introduce the spatio-temporal representation, a useful method to visualize the solutions $x(t)$ of systems with large delays or data from feedback experiment with a large time lag. We also explain the physical meaning of this tool using the autocorrelation function. Subsection. 2.3 reviews shortly the literature on discrete maps with large delays. Finally, we mention a formal, but significant interpretation of nonlinear delay systems as composition of two operators: the nonlinear function and a linear differential evolution scheme.

Section 3 describes the properties of various complexity measures and their scaling with time delay: Lyapunov spectrum, Floquet exponents, Kaplan-Yorke dimension, entropy, as well as the number of coexisting periodic solutions. Taking into account that the spectrum converges asymptotically to a continuous shape, the classification of instabilities is presented in Sec. 3.2 for large-delay systems, showing the similarity with that for spatially extended systems.

In Sec. 4, the applications of the multiple scale analysis to large-delay systems are given. In particular, it is explained how the normal forms can be derived for each particular type of instability. The physical discussion about the long-delay limit is provided in Sec. 5, where information propagation aspects, drift in the spatio-temporal representation, and boundary conditions are discussed.

Section 6 is devoted to the several spatio-temporal phenomena reported in the context of high-dimensional delay systems, such as spatio-temporal chaos, Eckhaus instability, stripes and square waves, strong and weak chaos, coarsening, nucleation, localized structures, spiral defects and turbulence.

The next Sec. 7 reports on the experiments on long-delayed systems, which are known to be mostly optical systems till now. Finally, we conclude with a summary and a discussion of future perspectives in Sec. 8.

2 Long-delay systems and spatio-temporal dynamics

The DDS (1) is an infinite-dimensional system, where the state is determined by the functions $x_t(\theta)$, $-\tau \leq \theta \leq 0$ that can be considered as "points" in the phase space. It is therefore natural to interpret the time interval of length τ as the *space(*-like) domain and try to map the problem to an evolution rule for the functions defined on this domain. A straightforward way of introducing the spatio-temporal coordinates is as $u(\theta, t) = x_t(\theta) = x(t + \theta)$, where θ plays the role of a spatial coordinate and t of a temporal one. In this case, the resulting dynamics is described by an equivalent transport equation (hyperbolic PDE with complicated boundary conditions), see Sec. 4.6 and system (45). However, the spatial variable defined in this way is, in fact, just a re-parametrization of the time t and the obtained PDE does not provide an additional physical insights into the dynamics. Therefore, we do not consider this representation except for a short description in Sec. 4.6.

Instead, here we concentrate on another spatio-temporal representation of the dynamics of system (1), when τ becomes large and the temporal and spatial variables can be defined in such a way, that they decouple from each other to some extent. The reason

behind such a decoupling is a difference in time scales, on which the new spatial and temporal variables are acting. We hope that this statement becomes more clear after the reading of the following sections. As a result of this representation, the obtained spatio-temporal system is simpler (usually of parabolic type) and allows to obtain additional insights in the properties of the system. Moreover, different systems with feedbacks, when the propagation times in the feedback loops are significantly larger than their natural time-scales, show common features that can be described in a unified way leading to some kind of normal forms.

In this section, we introduce and discuss the main ideas behind the spatio-temporal representation, focusing on its physical interpretation; more general comments on the consequences of the method are presented in Sec.5 while n Sections 3 and 4, more theoretical details and derivations will be given.

2.1 The spatio-temporal representation

The heuristic equivalence of DDS's with 1D, spatially extended systems can be pushed further with the aid of the following example, based on the Stuart-Landau delayed equation [44]:

$$\frac{dx}{dt}(t) = \mu x(t) + \nu |x(t)|^2 x(t) + \eta x(t-\tau). \tag{2}$$

System (2) was introduced to describe phenomenologically the oscillations of the emitted intensity from a CO_2 laser, in a setup with delayed, optoelectronic feedback on the losses. It is a modification of the normal form equation for the Andronov-Hopf bifurcation, with an extra additive, linear delayed coupling to keep in account the feedback at the lowest order.

Let us consider the temporal series depicted in Fig.1(a), obtained from a numerical integration in a chaotic regime with a delay time $\tau \gg 1$. Partitioning the time series in slices of length τ (with an arbitrary choice of the initial point), it appears that a certain degree of coherence is maintained between the value of the solutions at corresponding points (times) within consecutive slices. To better evidence such a behaviour, the slices can be plotted in a two-dimensional arrangement (Fig.1(b)). The horizontal axis can now be naturally interpreted as a *space*-like variable, indexing the variable spanning a delay-long cell. The role of a *time*-like variable is played by the integer numbering the slices.

Formally, the solution can be expressed as a function of a new set of independent variables (σ, θ) according to

$$t = \sigma + \theta\tau, \tag{3}$$

where $\sigma \in [0, \tau)$ is the *pseudo-space* and $\theta = 0, 1.2, ..$ the *pseudo-time*. We remark that the values of the solution are not affected by the use of the new variables, it is only a different parametrization of the independent variable t . The description of the solution based on (3) has been named Spatio-Temporal Representation (STR) [30, 43, 51, 52]. We remark that, since the STR is a re-organization of samples collected sequentially in

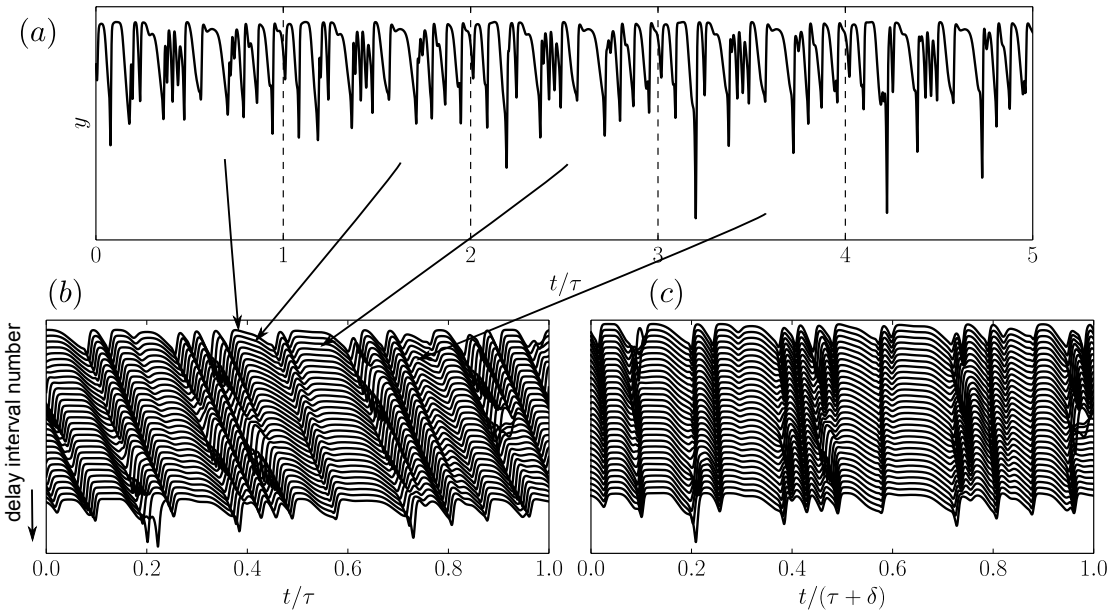

Figure 1: Illustration of the spatio-temporal representation and the drift. A trajectory of system (2) with $\tau = 100$, $\mu = 1 + i$, $\eta = 1.2$, and $\nu = -0.1 - 0.22i$ is shown in panel (a). Panel (b) shows consecutive pieces of length τ of the trajectory plotted one under another. (c) shows the same figure as (b) but with a slightly enlarged lengths $(\tau + \delta)$ of the intervals. For an appropriately chosen δ (the drift), the vertical correlation is maximal.

time, it can be applied as well to data from experiments where it can provide very useful insights.

As shown in Fig.1, the propagation of structures (cellular pattern) is evident in such representation, very similarly to what observed e.g. in coupled map lattices and in 1D spatially extended system such as the Complex-Ginzburg Landau (CGL) model.

The inspection of Fig.1(b) also reveals the existence of a *drift*: the pattern in a slice (almost) reappears in the successive slice shifted by some value δ. This feature is typical of DDS's and it is a consequence of the causality principle (we will return to this point in Sec. 5). The use of a slightly modified representation, with the interval size $\tau' = \tau + \delta$ (Fig. 1(c)) corresponds to the correct choice of a comoving reference frame and allows to obtain an almost vertical propagation. As seen in the following, the value of the drift δ can be found by studying the autocorrelation properties of the solution, namely, the highest peak of the autocorrelation function is at $\tau + \delta$.

2.2 Autocorrelation analysis

The STR described in Sec. 2.1 can be justified by the analysis of the normalized autocorrelation function

$$r(\xi) = \frac{\langle \bar{x}(t)\bar{x}(t-\xi)\rangle}{\sigma_x^2}, \tag{4}$$

where $\langle\cdot\rangle$ denotes time average, $\bar{x} = x - \langle x\rangle$, and $\sigma_x^2 = \langle \bar{x}^2 \rangle$.

The function r is a standard tool for extracting important features of the dynamics from a time series. It is proven to be very useful when the state of a system is known to a limited extent, e.g. in the case of data obtained from numerical integration of complex models or from experiments.

The autocorrelation for a chaotic signal from Eq. (2) with large delay is plotted in Fig. 2, showing many sharp peaks (revivals), nearly at the multiples of τ. They indicate the existence of temporal patterns almost repeating after a delay time, resulting in the pseudo-time cellular structure in the STR. As an effect of the chaotic dynamics, the height of the peaks is exponentially decreasing, and their decay time (measured in units of the delay time) gives an estimation of the average propagation length of the patterns in the pseudo time. A more accurate inspection reveals that the peaks are located at multiples of $\tau' = \tau + \delta$ and that the patterns are therefore drifting in the STR as noted before. The decay time t_c of the first peak at $t = 0$ (see Fig. 2), is instead a measure of the average coherence length in the pseudo space of such patterns. The above mentioned decays in the autocorrelation can be interpreted as a signature of a (pseudo-) temporal and (pseudo-) spatial disorder respectively.

Even if other methods based e.g. on mutual information or fractal dimension indicators are more powerful in the characterization of the dynamics, the autocorrelation permits to identify the variables to use for the STR. The multiple time scale analysis, as discussed in the following sections, is a natural extension of this analysis and allows to put on a rigorous ground the above considerations.

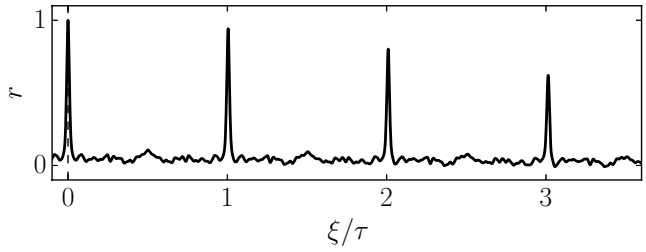

Figure 2: Autocorrelation function of a chaotic signal from the integration of (2) with $\tau = 100$, $\mu = -1 + i$, $\eta = 1.9$, and $\nu = -0.1 - 0.4i$.

Since the system cannot respond (change significantly) on times shorter than the coherence time, a rough estimation of the number of spatial degrees of freedom can be heuristically evaluated by the number of t_c within the delay interval, i.e. $\rho = \tau/t_c$ [36, 35, 38]. Such a conjecture is supported by the observation that t_c is often independent of τ in the limit of large delays. This is consistent with the reports that the attractor dimension scales linearly with τ [15]. It should be noted that the existence of a finite, non zero t_c implies a limit in the maximal amount of "information processed" by the delay system. In rigorous terms, attractors in DDS's are shown to have finite dimension [23].

It is common to define "long"-delay systems as those with $\rho \gg 1$, and it should be remarked that t_c is not an "instantaneous" time-scale of the system (i.e., in the absence of feedback), but a property of the delayed dynamics. On the other hand, t_c is indeed often close to the instantaneous time-scale in practice.

The sign of the peaks of the autocorrelation provide other important information about the system, related to the phase of the feedback signal. An example is shown in Fig.3, in the case of a delayed logistic map [38]. Negative revivals indicate out-of-phase coherent structures contributing to the autocorrelation. It should be noted that revivals are peaks in the *envelope* of the autocorrelation function: possible oscillations with negative values at higher frequencies are specific of the signal itself but do not carry information about the propagation. The difference is very much the same as for the group and phase velocities of wave signals. The case of negative revivals at the odd multiples of the delay time [39, 53] can be represented with a suitable STR, where the spatial cell is two- or more delays long. We will return to this point in Sec. 6.3.

The autocorrelation function can be shown to obey, in the case of linear DDS's, the same equation as the original signal. Given the system

$$\frac{dx}{dt}(t) = \mu x(t) + \eta x(t-\tau), \tag{5}$$

the equation for the autocorrelation function [54] reads as well

$$\frac{dr}{d\xi}(\xi) = \mu r(\xi) + \eta r(\xi - \tau). \tag{6}$$

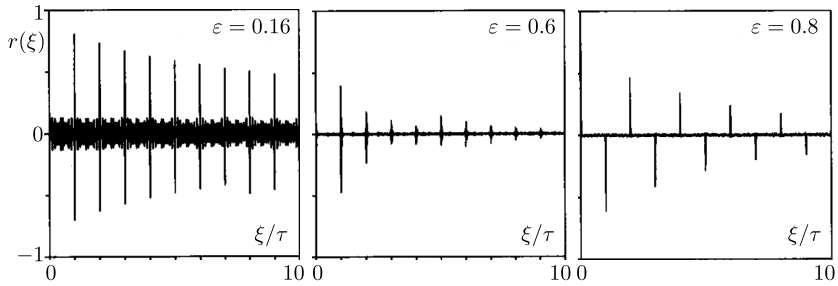

Figure 3: Autocorrelation functions for the delayed logistic map. (The figure is adapted with permission from Ref. [38]. Copyrighted by the American Physical Society.)

However, the initial condition for the evolution of the autocorrelation $r(\xi)$, $-\tau < \xi \leq 0$ depends on the whole dynamics $x(t)$ and need not be the same as the initial condition $x(t)$, $-\tau < t \leq 0$ for the linear system (5). As a result, the exact behavior of $r(\xi)$ and $x(t)$ can be different. Nevertheless, Eq. (6) indicates that the values of the autocorrelation in the following delay intervals, corresponding to separations larger than τ, are completely determined by the previous ones, and this dependence has the same properties as the properties of the solution itself, i.e. the STR holds for $r(\xi)$, the value of the drift is the same, etc.

The discussion above is rigorously valid for the linear model only. However, one could expect that a similar behavior is observed in more complicated situations. The autocorrelation has shown to be very useful also in experiments [55, 54]; a STR description for the autocorrelation can be derived from experimental data [55]. In this case, the averaging process is very effective in improving the signal-to-noise ratio and allows to obtain better results for, e.g., an estimation of the drift.

In setups with multiple feedback terms with different delays, the structure of the peaks of the autocorrelation function can be more complicated, reflecting the role of the multiple timescales involved. A STR is possible in this case also, with a proper choice of the variables and taking care of the drift over all components. We will discuss this topic in Secs. 4.4 and 6.8.

2.3 The discrete case: maps with long delay

Although the main emphasis of this manuscript is on time-continuous DDS, this section briefly reviews some results on the delayed maps. Iterated maps is a large and important class of dynamical systems with discrete time. The idea of a discrete dynamics with non-local feedback emerged early in the discussions on numerical integration of DDS's [15] and then they were studied by themselves as simple but very general systems.

Willeboordse [51] studied a map with delay as an alternative, algorithmic description of a Coupled Map Lattice (CML), providing similar behaviors. Indeed, he proposed a method to derive a delayed map from a CML, as a convenient method to obtain numerically the same "bulk" dynamics. The mapping between the two systems is a first example of pseudo spatio-temporal (in fact, called time-time) representation (Fig. 4).

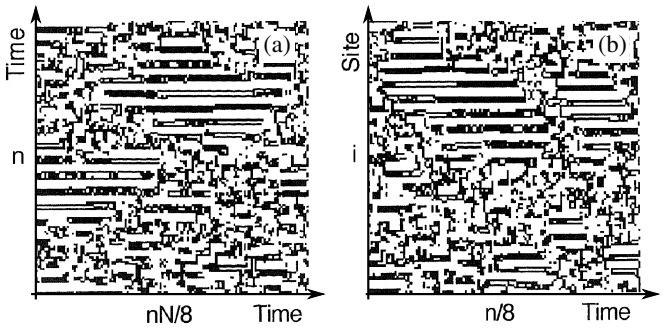

Figure 4: Time-time diagram for the time delayed map (a) and space-time diagram for the coupled-map lattice (b); every eighth step in the x-direction was plotted. (From [51]: Time-delayed map phenomenological equivalency with a coupled map lattice, F. H. Willeboordse, Int. J. of Bifurcations & Chaos 2, 721, Copyright @ 1992 World Scientific Publishing Co., Inc.)

He noticed also that the different boundary conditions may play an essential role in some cases.

After the introduction of the STR, long delayed maps were first investigated in [38, 56, 39]. The studies were motivated both by the experiments in a CO_2 laser with delayed [57] and long delayed [43] feedback on the losses, and from the growing interest in CML's [58, 59, 60].

In [38] two classes of delayed maps are discussed. The first (named class-I), is the discretization obtained e.g. by implementing the forward Euler integration scheme of the model

$$\frac{dy}{dt}(t) = -y(t) + F(y(t-\tau)) \tag{7}$$

including the Mackey-Glass [1] and Ikeda [4] delayed equations. Its peculiarity is that the local damping term is strictly negative, with important effects on the type of the dynamics in the large delay limit.

The second class has the form

$$y_{t+1} = (1-\varepsilon) f_1(y_t) + \varepsilon f_2(y_{t-T}), \tag{8}$$

which is not a discretized version of some differential equation, but is more general, with some nonlinear functions f_{12} and ε measuring the relative weight of the delayed coupling. Here T is an integer delay time; in the case of class-I systems it can be obtained from $T = \tau/t_c$ as discussed in Sec. 2.2. Using both the Bernoulli and logistic map nonlinear functions, the scaling of Lyapunov spectrum, fractal dimension, and Kolmogorov-Sinai entropy with the delay time is studied in [38] for different values of the parameter ε.

For systems (8), the temporal evolution of small perturbations δy_t is described by the linearized map

$$\delta y_{t+1} = (1-\epsilon) f_1^{'}(y_t)\delta y_t + \epsilon f_2^{'}(y_{t-T})\delta y_{t-T}. \tag{9}$$

Assuming a finite growth rate of δy_t, e.g. $\delta y_t \sim \mu^t$, $|\mu| > 1$, in the limit $T \to \infty$, the retarded term $\delta y_{t-T} \sim \mu^{-T}\delta y_t$ can be neglected. In this case, the maximum Lyapunov exponent is given by

$$\lambda_{max} = \ln|\mu| = \left\langle \ln|f_1^{'}(y_t)| \right\rangle + \ln(1-\varepsilon). \tag{10}$$

This approach is self-consistent and holds only if $\lambda_{max} > 0$. The exponent was named *anomalous*, to underline its different behavior in the large delay limit with respect to the rest of the spectrum. The anomalous exponent describes a fast decorrelation of the dynamics on short time scales, implying that the STR cannot be used: the information about the pattern in the previous delay time is lost. It was also pointed out that class-I systems cannot have an anomalous exponent, because of the negative instantaneous damping. However, it could be found in more complex setups, such as models with a larger number of coupled variables or experiments. The topics has been increasingly studied in discrete as well in continuous systems and in experiments [61, 62, 47, 63, 48, 64, 65, 66, 67, 68, 69, 70, 71, 72], and the terms *strong chaos,* when the anomalous exponent exists, and *weak chaos* has been introduced, remarking the difference between the two states. This point will be treated in details in Sec. 3 (general properties of the spectrum) and Sec. 6.4 (strong and weak chaos).

Apart from the anomalous contribution, the Lyapunov spectrum has been shown to scale with $1/T$ confirming the findings in differential-delay equations [15, 34]. From the knowledge of the spectrum both the Kolmogorov-Sinai (or metric) entropy and the fractal dimension can be calculated. This will be done in Sec. 3.6. As a result, it is found that the dimension grows linearly with delay T (exactly as it was found in CML's) allowing to identify the delay T as an effective system size. The only remarkable exception is the presence of an anomalous exponent, which upon rescaling is a diverging quantity; the connection with CML's fails in this case.

The role of (pseudo) spatio-temporal chaos in determining nonequlibrium statistical properties is reported in [56], in the case of a class-II type model based on logistic maps i.e. $f_1(x) = f_2(x) = \mu x(1-x)$ where $x \in [0,1]$. In this work, it is described and characterized the appearance of a phase transition mediated by chaotic defects in the STR, between a laminar and a turbulent regime with defects creation, annihilation and diffusion. The measured scaling exponents at the transition are in good agreement with those found in the CML's.

The statistical properties of the bidimensional patterns generated by the dynamics might depend on the choice of the updating rule and/or of the boundary conditions, even if the large aspect ratio (or delay) limit is achieved. In the case of class-II models, an investigation was reported in [39]. The evolution equation for a generic delayed map $x_{n+1} = F(x_n, x_{n+1-T})$ in the STR $n = s + tT$ can be written as

$$y_s^{t+1} = F(y_{s-1}^{t+1}, y_s^t), \tag{11}$$

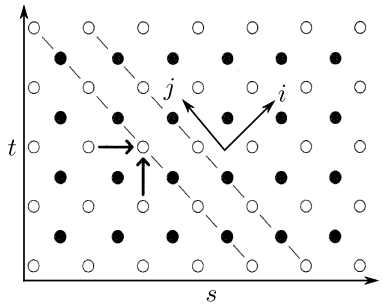

Figure 5: Coupling scheme for the map (11). Coordinates (s, t) correspond to the STR, while coordinates (i, j) of the tilted reference frame allow to rewrite the map as an extended, discrete system using two sub-lattices (empty and filled dots). (The figure is adapted with permission from Ref. [39]. Copyrighted by the American Physical Society.)

with the boundary condition $y_0^{t+1} = y_T^t$. The updating rule is clearly sequential, since we must proceed from $s = 1$ to T. In the representation (11) the coupling becomes local and the system is in the class of 1D extended systems. Considering the pattern generated by the rule (11), a different coordinate systems on it can be chosen by introducing a reference frame rotated by $\pi/4$ (see Fig. 5). Every point can be parametrized with the integers $i = s + t$ and $j = s - t$. Denoting the new variable as z_j^i, the map reads as

$$z_j^{i+1} = F(z_{j-1}^i, z_{j+1}^i); \tag{12}$$

the lack of the term z_j^i in the coupling implies the existence of two sub-lattices (depicted in Fig. 5 by empty and, respectively, filled circles). This case appears analogous to what found in CML's for $\varepsilon = 1/2$; however, boundary conditions and symmetries here are radically different.

Considering three different rules to generate the same pattern, such that the dynamical equations are the same but the boundary conditions are different, the authors of [39] investigated the behavior of the statistical indicators as a function of the coupling parameter. They found that the Kolmogorv-Sinai entropy density (i.e. the entropy divided by the delay) does not depend on the rule, and, hence, it may be associated to the pattern. The Kaplan-Yorke dimension density, as a consequence of the same property of the Lyapunov spectrum is instead rule dependent, and, hence, the diverse generated patterns show a different number of degrees of freedom.

The case of discrete, stochastic processes with two-delays is similarly analyzed in [73]. There, a time series evolving according to a nonlocal update rule can be mapped onto a local process in two dimensions with special time delayed boundary conditions.

The transition to chaos synchronization in networks of iterated maps in the limit of large delay times has been investigated in [64, 74]. In particular, in [74], general arguments about the dynamics of such a network predict a jump of the Kaplan-Yorke dimension of the chaotic attractor when the network synchronizes. In addition, the Kolmogorov entropy can show a discontinuous slope. This stays in accordance with

the fact, that the synchronization is related to the bifurcation transition, at which the dynamics starts to be confined to some low-dimensional synchronization manifold. As a result, the Kaplan-Yorke and the correlation dimension jump to a lower value when the network synchronizes.

2.4 Long delay dynamics as composition of operators

A formal decomposition of the class of models (7) was presented in [75]. There, it was pointed out that the dynamics can be formally described as the action of two successive operators on the solution in the segment $(0, \tau)$:

$$y_d \to z_d = F(y_d), \quad z_d \to y = \mathcal{L} z_d. \tag{13}$$

The first operator is a nonlinear transformation at every point (i.e., it is a local operator in the pseudo space), playing the same role of the nonlinear function in the CML's. The second is a linear operator, combining the differential operator and the (pseudo) time evolution from a delay to the successive one. The operator $\mathcal{L}$ can be written in the Fourier space as

$$y(k) = \frac{z_d(k)}{1 + ik}, \tag{14}$$

where k is the spatial wavevector, and approximated up to the second order by

$$y(k) \approx z_d(k) e^{-ik} e^{-k^2/2}. \tag{15}$$

It is apparent from (15) that $e^{-ik}$is responsible for the drift from a delay to the successive one, and the Gaussian factor describes a diffusion process. Simulations showed a good agreement of such an interpretation with a direct numerical integration of the original model. The class (7) can be thus described as an intermediate type between space-extended systems (due to the action of drift and diffusion in the pseudo space) and maps (iteration via a nonlinear local function).

3 Lyapunov spectrum and other dynamic indicators

In this section, we discuss the Lyapunov spectrum (see e.g. [76]) and other important dynamical indicators used for the analysis of delayed models. Particularly, we show how for long delays the spectrum splits into a pseudo-continuous part and another, finite set of exponents. This fact constitutes the theoretical foundation for the observation that the long-delay systems incorporate the properties of both spatially extended and finite-dimensional dynamical systems. The properties of pseudo-continuous spectrum allow to provide a universal classification of instabilities of long-delayed systems in analogy to the spatially-extended systems, as discussed in Sec. 3.2. The case of several hierarchical time delays is studied in Sec. 3.3. In Sections 3.4 and 3.5, the Floquet and Lyapunov exponents (LE) of periodic and, respectively, chaotic solutions are considered. Finally,

we discuss in Sec. 3.6 the scaling of the entropy and Kaplan-Yorke dimensions of the attractors in delayed systems.

3.1 Spectrum of long-delay systems

The dynamics in a close vicinity of any solution $s(t)$ of delay system (1) and its stability properties are determined by the linearized system

$$\frac{dx}{dt}(t) = A(t)x(t) + B(t)x(t-\tau), \tag{16}$$

where $A(t) = \partial_1 F(s(t), s(t-\tau))$ and $B(t) = \partial_2 F(s(t), s(t-\tau))$ are the derivatives (Jacobians) with respect to the first and the second arguments, respectively. When the considered solution is stationary $s(t) = s_0 = \text{const}$, the matrices A and B are constant, and the properties of (16) are described by the solutions of the characteristic equation

$$\det\left[-\lambda I + A + Be^{-\lambda\tau}\right] = 0. \tag{17}$$

Here I is the identity matrix. Equation (17) is a quasi-polynomial, which, in general, possesses infinitely many complex solutions. According to the general theory [77], they all are bounded from the right, i.e. $\mathrm{Re}\lambda < C$ and accumulate solely at $-\infty$. Hence, only finitely many roots of (17) determine the stability. In particular, if there are roots with $\mathrm{Re}\lambda > 0$, then the steady state s_0 is unstable, and if all roots have $\mathrm{Re}\lambda < 0$, then it is asymptotically stable with the exponential convergence rate $\exp((\mathrm{Re}\lambda)_{\max} t)$.

These basic properties of the spectrum already manifest some remarkable features of the delay-systems. The infinite-dimensionality is expressed by the infinite number of the characteristic roots λ. However, only a finite number of them play a decisive role for the dynamics, since the remaining part of the spectrum accumulates at $-\infty$ and corresponds just to an exponential (or sometimes even faster) decay. This will also be reflected in the properties of periodic solutions, as well as chaotic attractors. Roughly speaking, delay-equations is an example of an infinite-dimensional system, that demonstrates finite-dimensional phenomena in practice. The question is, how large the dimensionality of the observed phenomena can be: as we will see in the following, such a dimension can achieve any finite value and, in many cases it grows linearly with the time delay τ.

Coming back to the characteristic equation (17), an important question is therefore how many multipliers are important for the dynamics, or how many unstable multipliers may occur in the system. May it happen that their number becomes extremely large so that the system will start to exhibit essentially infinite-dimensional properties? The answer to this question is affirmative, and such a situation occurs when the time delay τ becomes large. Moreover, the number of "important" characteristic roots grows linearly with τ. An illustration of this situation is shown in Fig. 6, where the roots of a scalar characteristic equation are shown for three different values of time delay.

It is shown in [66] that the major part of the roots of (17) are converging to the following curves in the complex plane

$$\lambda = \frac{\gamma(\omega)}{\tau} + i\omega \tag{18}$$

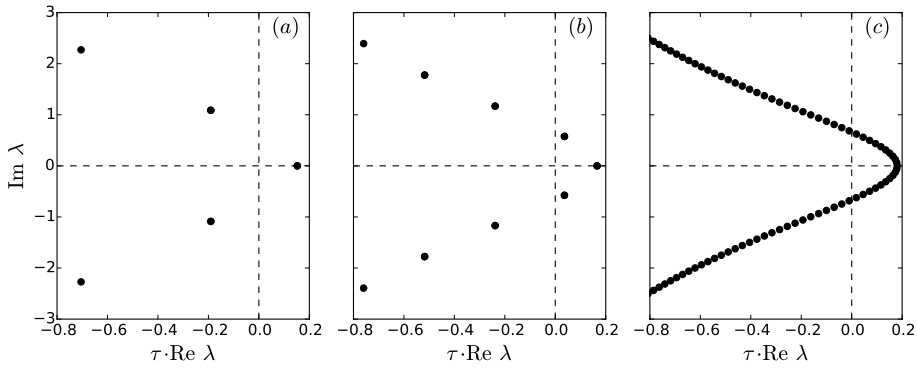

Figure 6: Spectrum of the scalar delay system $x' = ax(t) + bx(t-\tau)$ with $a = -1$ and $b = 1.2$. As τ increases from (a) to (c), the number of critical characteristic roots increases linearly and fill the curve of the pseudo-continuous spectrum (18). Delay values: $\tau = 5$ (a), $\tau = 10$ (b), and $\tau = 100$ (c). Remark that the real part is multiplied by τ.

with the real parts scaled as $1/\tau$. By substituting (18) into Eq. (17) and considering a leading order, it is easy to find that

$$\gamma(\omega) = -\ln|Y(\omega)|,$$

where $Y(\omega)$ is a root of the polynomial

$$\det\left[-i\omega + A + BY\right] = 0.$$

For instance, in the scalar case used in Fig. 6

$$\frac{dx}{dt}(t) = ax(t) + bx(t-\tau), \tag{19}$$

this curve is given by

$$\gamma(\omega) = -\ln\left|(i\omega - a)/b\right|, \tag{20}$$

and it has one maximum at $\omega = 0$ independently of the choice of the parameters a and b.

Although these curves are continuous, the spectrum, which converges to them is discrete with the distances between the neighboring characteristic roots scaling as $2\pi/\tau$. Moreover, the number of such curves is proportional to the number of variables on which the delayed feedback is acting. To be more specific, it is equal to the rank of the matrix B. Further details on the spectrum for the steady states can be found in [17, 77], and, for large delays in [45, 78, 63, 67, 49].

Another part of the spectrum is unstable and it is close to the unstable characteristic roots of the instantaneous system, i.e. the eigenvalues λ_A of the matrix A with positive real parts. For long delay, λ_A approximates a characteristic root of the delayed system

and leads to the instability. Such spectrum is also called strongly unstable [66] or anomalous [45], and it contains only a finite number of roots (or empty) that is equal to the number of unstable eigenvalues of the matrix A.

Summarizing, the spectrum of systems with long delays, with increasing delay starts to resemble the spectrum of spatially-extended systems, where the curves of the pseudo-continuous spectrum are analogous to the so-called dispersion-relation curves [79, 80]. On the other hand, the characteristic roots are discrete as in spatially-extended systems on a bounded spatial domain.

3.2 Classification of instabilities in systems with long delays

The destabilization in systems with long time delays can not be adequately described by individual local bifurcations (e.g. Hopf) when a pair of characteristic roots crosses the imaginary axis, but rather crossing of the families of characteristic roots located along a branch of the pseudo-continuous spectrum. The interplay of all Hopf bifurcations produces essentially high-dimensional phenomena, which are typical for spatially-extended systems. Figure 7 illustrates the main (codimension-1) destabilizations that may occur [63]. They can be classified into uniform, wave, and modulational, depending on the way the pseudo-continuous spectrum crosses the imaginary axis. This classification is inspired by the corresponding classification existing in PDE systems [79].

Uniform instability occurs when the spectrum is tangent to the imaginary axis at $\omega = 0$, see Fig. 7(a). The generic crossing in this case is quadratic. The simplest model where such an instability is present is the scalar equation (19). In fact, this is the only instability that may occur for steady states in the scalar case (19) with real coefficients, since the pseudo-continuous spectrum has always the maximum at $\omega = 0$ in this case, see [49]. Fig. 7(a) was calculated for $a = -1$, $\tau = 50$, and the b parameters as indicated in the figure. The dashed line shows the pseudo-continuous spectrum line given by (18) and (20).

Wave (or Turing[2]*)* instability happens when the crossing takes place at $\omega \neq 0$, see Fig. 7(b). For such an instability of steady states to occur, at least two variables should be present in the system. The simplest equation possessing the aforesaid instability is the complex-valued, scalar equation (19) with complex coefficients. Figure 7(b) was obtained for $a = -1 + i$ and $\tau = 50$.

Modulational instability is generic for the destabilization of systems with symmetry or periodic solutions, where a zero characteristic root appears naturally and persists for all parameter values, see Fig. 7(c). Similarly to wave-instability, several (i.e. more than one) variables are needed in order to observe it.

The above mentioned instabilities play often a fundamental role in the appearance of various nonstationary patterns [46, 62, 48, 63, 81, 49, 82], and, in the following sections we will mention them in the contexts of emerging spatio-temporal phenomena.

[2] It seems that there is still no common agreement about how to call this instability. In some previous publications, also by the authors, the name Turing instability was used. Here, we use the name "wave instability", since it seems to be more appropriate for this case.

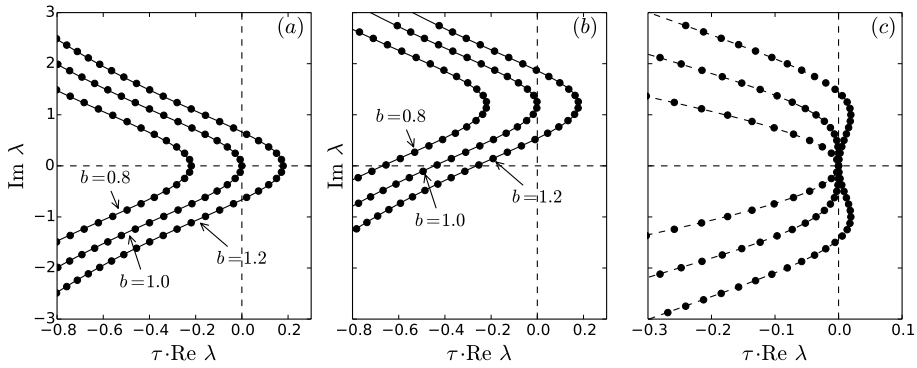

Figure 7: Classification of instabilities in large-delay systems. From left to right: uniform, wave (Turing), and modulational.

3.3 Spectrum in systems with multiple hierarchical time delays

In the case of multiple hierarchical time delays $1 \ll \tau_1 \ll \tau_2 \ll \cdots \ll \tau_n$, the spectrum can also be divided into various components, which correspond to each timescale τ_i [83, 84, 85, 67]. For instance, in the case of the system with two delays

$$x' = Ax(t) + B_1 x(t-\tau_1) + B_2 x(t-\tau_2),$$

the τ_1-spectrum has still the form of a one-dimensional pseudo-continuous spectrum. However, the destabilization in such systems is governed generically by the τ_2-spectrum, which scales as

$$\lambda = \frac{\gamma(\omega,\varphi)}{\tau_2} + i\omega, \quad \varphi = \left(\frac{2\pi\omega}{\tau_1}\right) \bmod 2\pi,$$

and it is asymptotically located on a two-dimensional surface $\gamma(\omega,\varphi)$, which can be found explicitly as

$$\gamma(\omega,\varphi) = -\ln|Y(\omega,\varphi)|, \; Y \text{ satisfies } \det\left[-i\omega I + A + B_1 e^{i\varphi} + B_2 Y\right] = 0. \tag{21}$$

As a result, the destabilization is characterized by a family of characteristic roots laying on a surface, just as in the case of a two-dimensional dispersion relation in spatially-extended systems. Example of such a destabilizing surface is shown in Fig. 8. More details can be found in [83, 84, 85, 67], where, in particular, the interplay between different types of spectra is explained.

When the number of delays is k, the destabilization is governed by a k-dimensional surface [83].

As a result, in systems with hierarchical time delays, various spatiotemporal phenomena can be observed, which are similar to those in spatially-extended systems with higher number of spatial dimensions. Examples of such phenomena, 2D spirals and defect turbulence, will be given in Sec. 6.8.

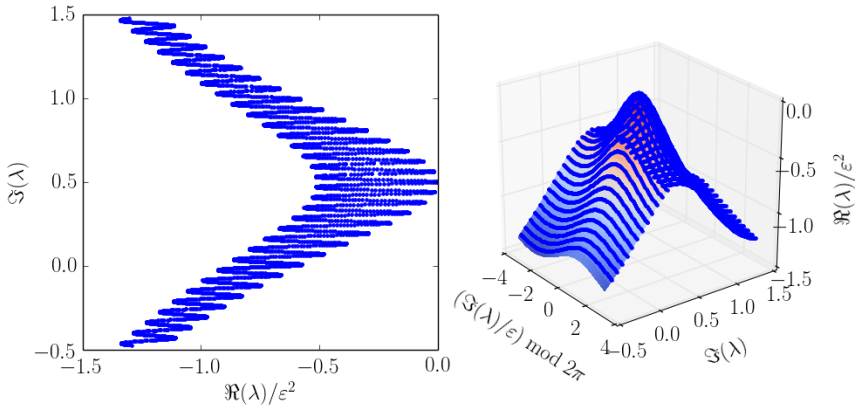

Figure 8: Example of the spectrum for system $x' = ax(t) + bx(t-\tau) + cx(t-\tau_2)$ with $a = -0.4 + 0.5i$, $b = 0.1$, $c = 0.3$, $\tau_1 = 100$, and $\tau_2 = 10^4$. Points denote the characteristic roots computed numerically. The right panel shows the surface of the 2D pseudo-continuous spectrum, which is given analytically by the function (21), together with the numerical points.

3.4 Scaling of the Floquet exponents of periodic solutions

The scaling properties of the steady states spectrum discussed in the previous section, hold for periodic solutions as well [47, 86]. Given a periodic solution $s(t)$ of system (1), the linearized equation around this periodic solution has the form (16) with periodic matrices $A(t)$ and $B(t)$. The Floquet exponents λ measure the exponential growth of small perturbations from this periodic solution, i.e. the growth rate of the solutions of the linearization (16). In particular, it is known [77] that for any Floquet exponent λ there is a solution $x(t)$ of the linearized equation such that $x(t) = e^{\lambda t}p(t)$ with periodic $p(t)$. The inverse is also true.

As it is shown in [47, 86], the spectrum of Floquet exponents converges for large delays asymptotically to curves with the same asymptotic properties (18) found for steady states, with real parts scaling as $1/\tau$. For periodic solutions, an additional consideration is needed to explain the meaning of the large delay approximation. In contrast to steady states, which are independent on time delay and solve the equation $F(s, s) = 0$, the periodic solutions $s(t) = s(t + T)$ are changing their shape and period T when the delay τ is changed. However, due to the periodicity of $s(t)$, it holds $s'(t) = F(s(t), s(t - \tau_0)) = F(s(t), s(t - kT - \tau_0))$, and, hence the same periodic solution $s(t)$ exists for all delay values $\tau = \tau_0 + kT$, $k \in \mathbb{Z}$. As a consequence, one can consider the stability of the solution $s(t)$ as the delay increases by steps of T.

From a practical point of view, the pseudo-continuous spectrum does provide a good approximation for the spectrum of Floquet exponents when the period of the periodic solution is much smaller than the time delay.

3.5 Scaling of Lyapunov exponents

As discussed above, the basic property of the spectrum of systems with long delays is the existence of families of LEs (resp. eigenvalues or Floquet exponents) that are asymptotically continuous. In the case of chaotic systems, this implies the appearance of so called weak chaos characterized by a set of unstable LEs, which scale as $1/\tau$, and their number is proportional to τ. As a result, extensive chaos, or, hyperchaos with large number of unstable dimensions arises [38, 65, 67, 68]. When instead the largest LE does not scale with τ, i.e. it is of order 1, strong chaos regime sets in.

The phenomena specifically associated with weak and strong chaos will be discussed later in Sec. 6.4. Here, we focus on the reasons for the appearance of the corresponding scaling of LEs. Formally, the LEs are defined as the growth rate of the perturbations for the linearized equation (16), where $A(t)$ and $B(t)$ are possibly irregular functions defined as Jacobians evaluated at a given orbit $s(t)$ within a chaotic attractor. The LEs computed from the truncated ODE system

$$\frac{dx}{dt}(t) = A(t)x(t) \tag{22}$$

play a special role. Note here that $A(t) = \partial_1 F(s(t), s(t-\tau))$ is still evaluated at the solution $s(t)$ of the full nonlinear delayed system (1). In [65, 69, 67, 68], they are called instantaneous or sub-Lyapunov exponents, or in [38], anomalous LE's.

In particular, when there is a positive sub-Lyapunov exponent $\lambda_s > 0$, it can be shown that there is a LE λ of the original delay system that is close to λ_s for long time delays. In this case, the maximal LE does not scale with time delay, and, hence, the perturbations $x(t)$ grow on a timescale $t \sim 1/\lambda_s$, which is smaller than the delay interval. This situation is called strong chaos, see Sec. 6.4, and the corresponding LE is called strongly unstable. It is straightforward to see the analogy between such a LE and the strongly unstable eigenvalues or Floquet multipliers for the case of steady states and periodic solutions mentioned in Secs. 3.1 and 3.4.

In the case when all sub-Lyapunov exponents are negative, the whole spectrum of LE's scales as $1/\tau$. This can be supported by the following reasoning [65] applied to the linearized equation (16). Let $t = \sigma + \tau j$, where $0 \le \sigma \le \tau$ and $j = \lfloor t/\tau \rfloor$ is the number of full delays τ within the interval of the length t. Denote $\xi_j(\sigma) := x(\sigma + \tau j)$. The linear equation (16) can be written with respect to ξ_j as follows

$$\frac{d\xi_j}{d\sigma}(\sigma) = A_j(\sigma)\xi_j(\sigma) + B_j(\sigma)\xi_{j-1}(\sigma), \tag{23}$$

where $A_j(\sigma) = A(\sigma + \tau j)$ and $B_j(\sigma) = B(\sigma + \tau j)$. Let $X(t, t')$ be the fundamental solution of the truncated system (22). Since we assume that all LE's of the truncated system are negative, we have that this fundamental solution is exponentially decreasing as $\|X(t,t')\| \le Me^{-\lambda_0(t-t')}$ with some positive constants M and λ_0. Using the fundamental solution X, the Eq. (23) can be solved with respect to $\xi_j(t)$ using the variation of constants formula

$$\xi_j(\sigma) = X_j(\sigma, 0)\xi_{j-1}(\tau) + \int_0^\sigma X_j(\sigma, \sigma')B_j(\sigma')\xi_{j-1}(\sigma')d\sigma', \tag{24}$$

where $X_j(\sigma,\sigma') := X(\sigma+\tau j, \sigma'+\tau j)$. From Eq. (24) and using the exponential decrease of X, one can obtain the following estimate

$$|\xi_j|_C \le L_j\,|\xi_{j-1}|_C \le (L_j \cdot L_{j-1} \cdot \cdots \cdot L_1)\,|\xi_0|_C\,,$$

where $|\xi_j|_C := \sup_\sigma |\xi_j(\sigma)|$ is the maximum of absolute value of the function $\xi_j(\sigma)$ on a j-th delay interval. In fact, the constants L_j are estimations of the upper bound of the absolute value of the fundamental matrix $|X_j(\sigma,\sigma')|$ of the truncated system on j-th delay interval (all possible σ and σ'). Assuming also that the properties of the chaotic attractor are in some sense "homogeneous" such that there is a bound L for all constants L_j, and the estimate

$$|\xi_j|_C \le L^j\,|\xi_0|_C$$

holds, we obtain

$$|x(t)| = |x(\sigma+\tau j)| \le |\xi_j|_C \le L^j\,|\xi_0|_C \le L^{t/\tau}\,|\xi_0|_C = e^{t\ln L/\tau}\cdot \text{const.}$$

The obtained estimate shows that the exponential grows rate of $x(t)$ and, hence, the LE, scales at most as $1/\tau$ for the case, when no strongly unstable LEs are present. We remark that the "homogeneity" assumption and the existence of a uniform bound for L_j can be made exact for the case of scalar DDS (1), see [49]. For the vector case, the above reasoning seems to be plausible; however a rigorous proof is still missing.

We should also mention earlier works on LEs for DDEs [15, 33, 36], where, in particular, the above scaling was observed.

3.6 Entropy and Kaplan-Yorke dimension

In this section, we shortly mention the consequences which follow directly from the scaling properties of the Lyapunov spectrum. We assume that the Pesin entropy formula for the metric entropy holds [87]

$$h_\tau = \sum_{\lambda_i>0} \lambda_i, \tag{25}$$

where the sum is taken over all positive LEs. The entropy is the result of the total asymptotic exponential rate of the expansion. In the case of DDS with long delays, the sum can be splitted into two terms. The first is for the strongly unstable spectrum (if it exists), and the second for the positive part of the pseudo-continuous spectrum

$$h_\tau = h_{su} + h_{pc} = \sum_{\text{str. unst.}} \lambda_{s,j} + \sum_{\substack{\lambda_i>0 \\ \text{pseudo-cont.}}} \lambda_i.$$

Here we assumed a generic situation when no critical spectrum occurs, i.e. there is no zero sub-Lyapunov exponent. Taking into account the scaling properties of each part of

the spectrum, we see that for a long delay the first part $h_{su} \to h^*_{su} = \text{const}$ for $t \to \infty$, and the second part

$$h_{pc} \to \sum \frac{\gamma_j}{\tau} \approx \int_{[0,\Omega_+]} \gamma(\omega) d\omega = h^*_{pc},$$

converges also to a constant, that equals to the integral of the (rescaled) asymptotically continuous spectrum on the range $[0, \Omega_+]$ where this spectrum is positive. The rescaled spectrum γ_j should be considered as a function of the variable $\omega = j/\tau$. Despite of the fact that the number of unstable LEs grows linearly with τ, their magnitude scales as $1/\tau$. As a result, this integral converges to a constant when $t \to \infty$.

As a result, with $\tau \to \infty$ the entropy converges to a constant value

$$h_\tau \to h_\infty = h^*_{su} + h^*_{pc},$$

which is composed of two contributions, one from the strongly unstable spectrum h^*_{su}, in the case of strong chaos (see Sec. 6.4), and another one (h^*_{pc}) for the contribution of the pseudo-continuous spectrum. Here the duality of the DDS as a bridge between spatially-extended finite-dimensional systems reveals again.

The Lyapunov dimension of an attractor can be evaluated using the well-known Kaplan-Yorke formula [88]

$$d_{KY} = k + \frac{1}{|\lambda_{k+1}|} \sum_{i=1}^{k} \lambda_i. \tag{26}$$

The integer k is the maximum value of l such that the sum $\lambda_1 + \cdots + \lambda_l$ is positive. The ordering $\lambda_1 \geq \lambda_2 \geq \cdots$ is assumed. Here again, the sum $\sum_{i=1}^{k} \lambda_i$ can be splitted into two parts: h_{su} (it is zero when no strong spectrum is present) and the sum over the interval $[0, \Omega_0]$ such that

$$h_{su} + \int_{[0,\Omega_0]} \gamma(\omega) d\omega = 0. \tag{27}$$

The value of k is then given by $\lfloor \Omega_0 \tau \rfloor$, and linearly grows with τ. Taking into account that the LEs are at the points i/τ, $i = 1, 2, \ldots$, we see that

$$\sum_{i=1}^{k} \lambda_i \approx h_{su} + \int_{[0,\Omega_0]} \gamma(\omega) d\omega + \left(\frac{\Omega_0}{\tau} - \left\lfloor \frac{\Omega_0}{\tau} \right\rfloor \right) \gamma(\Omega_0)$$

Since $\lambda_{k+1} \approx \frac{\gamma(\Omega_0)}{\tau}$, we finally obtain for the Kaplan-Yorke dimension the scaling

$$d_{KY} \approx \Omega_0 \tau$$

i.e. it grows linearly with the time delay, and $d_{KY}/\tau \to \Omega_0 = \text{const}$ for $\tau \to \infty$.

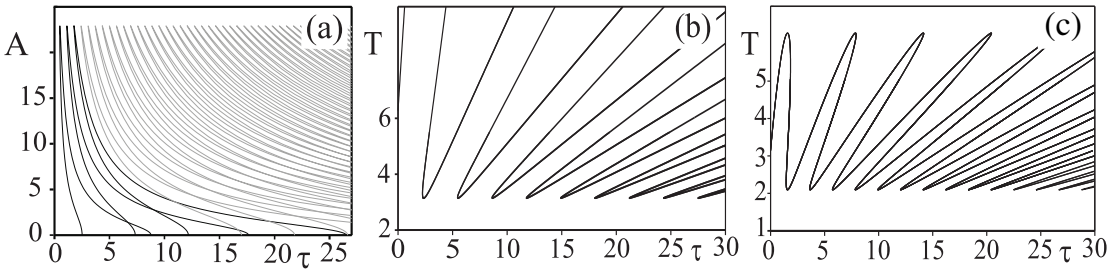

Figure 9: Typical "reappearance" of the branches of periodic solutions versus time delay τ. (a) Duffing oscillator (28) with delayed feedback; the amplitude A of the periodic solutions versus time delay τ is shown; parameters are $a = 0.5$, $b = 0.6$, and $d = 0.06$. (b)-(c) Oscillator (2) with parameters $\nu = -1$, $\eta = 1$, and $\mu = 2 + i$ for (b), $\mu = 2 + 2i$ for (c), respectively.

3.7 Growth of the number of coexisting periodic solutions with delay

An important complexity measure of a dynamical system is provided by the number of coexisting periodic solutions. It is shown in [47] that DDS (1) generically possess coexisting periodic solutions, the number of which grows linearly with τ. Typical examples are shown in Fig. 9, where the branches of periodic solutions are shown versus time delay. In particular, Fig. 9(a) corresponds to the Duffing oscillator with delayed feedback

$$x''(t) + dx'(t) + ax(t) + x^3(t) + b\,(x(t) - x(t-\tau)) = 0, \tag{28}$$

see the figure caption for the parameter values. One can observe how the branch is created in Hopf bifurcations, and how it "reappears" with a modified shape for larger delays. Similarly, Figs. 9(b) and (c) show branches of periodic solutions for the Stuart-landau oscillator (2).

In fact, such a reappearance is shown to be generic for systems with time delay [47]. It is a consequence of an elementary property of DDS such that any periodic solution $x(t)$ with a period $T(\tau)$, which exists for a time delay τ also exists (reappears) for the time delay $\tau + kT(\tau)$ with k being an arbitrary integer number. Moreover, the reappearing branches change their shape and stretch with the increasing of the delay, thus overlapping with each other, leading to the multistability. A proper counting of the number of such overlapping branches gives the following estimate for the number of coexisting periodic solutions

$$N \approx \kappa\tau = \left(\frac{1}{T_{\min}} - \frac{1}{T_{\max}}\right)\tau, \tag{29}$$

where $T_{\min}$ and $T_{\max}$ are the maximal and minimal period along each "elementary" branch. In the case when the period is unbounded, as in Fig. 9(b), this formula reduces to

$$N \approx \kappa_2\tau = \frac{1}{T_{\min}}\tau. \tag{30}$$

More details on the reappearance, the stability properties of the branches, as well as on some associated bifurcation properties (note a sequence of fold or Hopf bifurcations) can be found in [47]. Notice also that there may exist few primary branches, which cannot be mapped one onto another by the transformation $\tau \to \tau + kT(\tau)$. In this case, each branch will reappear increasing the delay time. The growth rate κ is here a superposition of the corresponding rates. Generally speaking, Eq. (29) gives a lower bound for the number of periodic orbits.

For DDS with an additional S^1 symmetry, e.g. the Stuart-Landau system, one can even show that the number of relative periodic solutions (called sometimes modulated waves, i.e. the solutions of the form $z(t) = e^{i\omega t}A(\beta t)$ with periodic $A(t)$) grows even faster, as τ^2 [89].

4 Multiple time-scale analysis and normal forms

In the previous sections we have shown that long-delayed systems are characterized by a natural separation between different timescales. This can be, in particular visualized by the space-time representation. A more quantitative analysis, employing the autocorrelation function as discussed in Sec. 2.2 can furthermore estimate the degree of coherence along such scales. In this section, we present and discuss the applications of multiple timescale analysis methods to different classes of long-delayed systems.

4.1 Reduction to normal form close to destabilization

We start by briefly discussing how the Ginzburg-Landau equation can be derived as a normal form close to a destabilization of a system with long time delays.

The reason why a parabolic partial differential equation (PDE) appears, instead of a standard, low-dimensional normal form as in the case of bifurcations in ODEs, becomes apparent when taking into account the shape of the spectrum of long-delay systems. As described in Sec. 3.1, the spectrum approaches asymptotically a set of continuous curves in the appropriately rescaled complex plane $(\tau \mathrm{Re}\lambda, \mathrm{Im}\lambda)$, see e.g. Fig. 7. As a consequence, the destabilization is governed by the crossing of the curves of the imaginary axis, similarly to the case of parabolic PDEs, where such curves are called dispersion relations. In the case of PDEs, the normal forms at some destabilizations are Ginzburg-Landau equations [79, 80], and the normal form equations depend only on the type of the destabilization and not on the details of the original equations.

It turns out that such normal forms can be derived for delay systems as well. However, while the spatial coordinates in the PDE case are naturally defined, in the delay case the role of the spatial coordinates in the normal form is played by different scales of the time εt, $\varepsilon^2 t$, etc.

4.2 Uniform instability

In this section, we give the main ideas for the derivation of the normal form using the simple example of system (1) with a scalar variable $x(t)$. A more detailed derivation

with a rigorous proof can be found in [49].

The main assumptions at the basis of the derivation are the following:
(i) There is a steady state x^*, which can be set to zero by a coordinate transformation.
(ii) The time delay is large $\tau \gg 1$. We exclude also the existence of other large parameters, or, equivalently, small parameters that are on the order of $\varepsilon = 1/\tau$ or smaller.
(iii) The steady state is close to a destabilization, i.e. the parameter values are such that the spectral curve is crossing or about to cross the imaginary axis, as depicted in Fig. 7(a). Since the pseudo-continuous spectrum (18) is given by the function $\gamma(\omega) = -\ln|(i\omega - a)/b|$ (shown in Sec. 3.1), the destabilization takes place for $a < 0$ and $|a| = |b|$. Here a and b are the derivatives of the right hand side with respect to the non-delayed, and delayed argument at zero, respectively. Hence, the parameters of the system should be close to this condition for the normal form to approximate the dynamics.
(iv) Finally, we assume that the nonlinearity is of the third order to exclude the case of transcritical bifurcation.

A general scalar delayed system, which satisfies the above conditions (i)-(iv) can be formally written as

$$x'(t) = \left(a + a_1\varepsilon^2\right) x(t) + (\pm a + b_1\varepsilon^2)x(t-\tau) + f(x(t), x(t-\tau), \varepsilon^2), \tag{31}$$

where the nonlinear function f is of the third order in $x(t)$ and $x(t-\tau)$. We also point out that the perturbations $a_1\varepsilon^2$ and $b_1\varepsilon^2$ are of order ε^2, since the amplitude of the solution emerging in the bifurcation scales as ε and, thus it will have a square root dependence on the perturbation, similarly to the case of the Hopf or pitchfork bifurcation [90].

Substituting now the general multiscale Ansatz

$$x(t) = \varepsilon u_1(\varepsilon t, \varepsilon^2 t, \varepsilon^3 t) + \varepsilon^2 u_2(\varepsilon t, \varepsilon^2 t, \varepsilon^3 t) + \cdots$$

into Eq. (31) and considering separately equations obtained for the terms with different orders of ε up to the order ε^3 (solvability conditions, excluding secular terms), one obtains the following result:

$$x(t) \approx \varepsilon A\left(\varepsilon t + \frac{1}{a}\varepsilon^2 t, \varepsilon^3 t\right),$$

where the function $A(x, \theta)$ of two variables satisfies the PDE

$$\partial_\theta A\left(x, \theta\right) = \frac{1}{2a^2}\partial_x^2 A\left(x, \theta\right) + \frac{1}{a^2}\partial_x A\left(x, \theta\right) - \frac{(a_1 \mp b_1)}{a} A\left(x, \theta\right) - \frac{\varsigma}{a} A\left(x, \theta\right)^3 \tag{32}$$

with the boundary condition

$$A\left(x, \theta\right) = \mp A\left(x - 1, \theta\right). \tag{33}$$

Here $\varsigma = \frac{1}{6}\left(f_{111} \mp 3f_{112} + 3f_{122} \mp f_{222}\right)$, and the sub-indexing of f denotes the partial derivatives with respect to the corresponding variables.

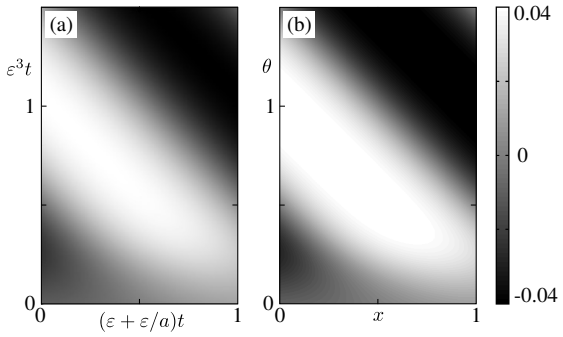

Figure 10: (a) Evolution for DDS (34) in the rescaled coordinates $x = \left(\varepsilon + \varepsilon^2/a\right) t$, $\theta = \varepsilon^3 t$. The magnitude of the solution $y(t)$ is shown by different scale of gray. (b) Evolution of the corresponding solution of the related amplitude equation (35).

The variable $x = \varepsilon t + \frac{1}{a}\varepsilon^2 t$ is called pseudo-space and $\theta = \varepsilon^3 t$ pseudo-time. Notice that in such a way the introduced pseudo-time and pseudo-space variables are in agreement with the geometric spatio-temporal description presented in Sec. 2.1. Indeed, the spatial domain $0 \le x \le 1$ corresponds to an interval of $0 \le t \le \frac{\tau}{(1+\varepsilon/a)}$, which is equal to τ apart for the small correction due to the drift.

Figure 10 shows an example for the scalar delay equation

$$y'(t) = -0.999y(t) - y(t-\tau) - 0.5y^3(t) \tag{34}$$

with $\tau = 100$. The solution is plotted in Fig. 10(a) using the spatiotemporal coordinates $x = \left(\varepsilon + \varepsilon^2/a\right) t$ and $\theta = \varepsilon^3 t$. Such a plot corresponds to the spatio-temporal representation discussed in Sec. 2.1. Figure 10(b) shows the corresponding solution of the related to (34) normal form

$$\partial_\theta A = \frac{1}{2}\partial_{xx} A + \partial_x A + 10A - \frac{1}{2}A^3, \quad A\left(x,\theta\right) = -A\left(x+1,\theta\right). \tag{35}$$

As seen in the figure, the similarity between the two solutions is a very high.

Further details on the derivation of the normal form (32)–(33) as well as a rigorous error estimate can be found in [49].

4.3 Wave instability in 1D

The wave destabilization takes place when the pseudo-continuous spectrum is crossing the imaginary axis at a non-zero frequency (see Sec. 3.2 and Fig. 7(b)). Such a situation cannot occur in the scalar case, since the pseudo-continuous spectrum there has a unique maximum at $\omega = 0$. In fact, at least two variables are necessary to observe the wave instability.

The simplest example of such a system is the scalar equation, with a complex variable z [46]

$$\frac{dz}{dt}(t) = (\alpha + i\beta)z(t) - z(t)|z(t)|^2 + z(t-\tau), \tag{36}$$

where α and β are real parameters. The pseudo-continuous spectrum for this system is given by the function

$$\gamma(\omega) = -\frac{1}{2}\ln\left[\alpha^2 + (\omega-\beta)^2\right],$$

which has a global maximum at $\omega = \beta$; hence, the wave destabilization occurs when α becomes positive and $\beta \neq 0$, see Fig. 7(b). Using a multiscale approach similar to that described in Sec. 4.2, the following normal form in the vicinity of this bifurcation can be derived [46]:

$$\partial_\theta A = \frac{1}{2}\partial_x^2 A + \partial_x A + \mu A - A\,|A|^2\,, \tag{37}$$

equipped with the boundary condition $A(x,\theta) = e^{i\varphi}A(x-1,\theta)$ with some phase φ. The relation between the solution $z(t)$ of the delay equation and $A(x,\theta)$ from the normal form is

$$z(t) \approx \varepsilon e^{i\beta t} A(\varepsilon t - \varepsilon^2 t, \varepsilon^3 t).$$

In contrast to the case of the uniform instability, the amplitude $A(x,\theta)$ is complex-valued and it is determined by the complex Ginzburg-Landau equation (37); it can therefore exhibit more complicated dynamical phenomena than the real normal form (32). Moreover, the amplitude A is now modulating the periodic "signal" $e^{i\beta t}$. One of the effects observed in such systems is the Eckhaus phenomenon, which will be discussed in Sec. 6.2.

4.4 Wave instability in 2D

A paradigmatic model describing the wave instability in two dimensions is provided by the equation similar to (36) but with two time delays, which are acting on different time scales [85, 84]:

$$\frac{dz}{dt}(t) = az(t) + bz(t-\tau_1) + cz(t-\tau_2) + dz(t)|z(t)|^2, \tag{38}$$

where a, b, c, and d are some complex parameters and $1 \ll \tau_1 \ll \tau_2$. To be more specific, it is assumed that $\tau_1 = 1/\varepsilon$ and $\tau_2 = \kappa/\varepsilon^2$ with a small parameter ε. The stability analysis of the linearized system leads to the following critical pseudo-continuous spectrum

$$\lambda = \lambda(\omega,\phi) = \varepsilon^2\gamma_2(\omega,\phi) + i\omega,$$

where its real part is determined by the two-dimensional function (surface)

$$\gamma_2(\omega,\phi) = \frac{1}{\kappa}\left[\ln|c| - \ln\left|i\omega - a - be^{i\phi}\right|\right] \tag{39}$$

(see Sec. 3.3). In addition, the following conditions should be satisfied: $\mathrm{Re}\,a < 0$ and $|b| < \mathrm{Re}\,|a|$; otherwise, the system is unstable with some stronger instability, i.e. with positive real part of the spectrum scaling as $\mathcal{O}(\varepsilon)$ or $\mathcal{O}(1)$. A straightforward analysis of the function (8) shows that it becomes positive when $\mathrm{Re}\,a + |b| + |c| > 0$. Hence,

one can introduce a natural destabilization parameter $P = \mathrm{Re}\, a + |b| + |c|$ with $P = 0$ determining the critical value.

In order to study the dynamics of the system close to this destabilization, the multiscale anazatz is used leading to the following relation [85, 84]

$$z(t) \approx \varepsilon A\left(\varepsilon^4 t, \varepsilon t - \nu\varepsilon^3 t, \varepsilon^2 t - \nu|b|\varepsilon^3 t\right),$$

where $\nu := -(a + |b|)^{-1} > 0$, the complex amplitude $A(\theta, x, y)$ depends on the slow pseudo-time $\theta = \varepsilon^4 t$ and on the two pseudo-spatial variables $x = \varepsilon t(1 - \nu\varepsilon^2)$ and $y = \varepsilon^2 t(1 - \nu|b|\varepsilon)$, each of them corresponding to the particular delay. In this way, x can be related to $\tau_1 = 1/\varepsilon$ timescale and y to the timescale $\tau_2 = \kappa/\varepsilon^2$ with some additional drift corrections given by the terms of ε^3 order. The amplitude A satisfies the normal form equation

$$\nu^{-1}\Phi_\theta = p\Phi + \nu|b|\Phi_x - \left(1 - \nu|b|^2\right)\Phi_y + \frac{\nu}{2}\left(\Phi_{xx} + 2|b|\Phi_{xy} + |ab|\Phi_{yy}\right) + d\Phi|\Phi|^2 \quad (40)$$

with the following boundary conditions

$$\Phi(x, y, \theta) = e^{i\phi_b}\Phi\left(x - 1, y, \theta\right), \quad (41)$$

$$\Phi(x, y, \theta) = e^{i\left(\phi_c - \phi_b\left\lfloor\frac{\kappa}{\varepsilon}\right\rfloor\right)}\Phi\left(x - (\frac{\kappa}{\varepsilon}\mathrm{mod}1), y - \kappa, \theta\right), \quad (42)$$

where $p = P/\varepsilon^2$ and $\lfloor\cdot\rfloor$ denotes the integer part of a number.

If the boundary conditions can be neglected, one can simplify Eq. (40) and eliminate the convective terms with Φ_x, Φ_y as well as the cross-derivative Φ_{xy}, using an appropriate coordinate transformation. The final equation has the simpler form:

$$\Phi_\theta = p\Phi + |a|^{-1}\left(\Phi_{xx} + \Phi_{yy}\right) + d\Phi|\Phi|^2, \quad (43)$$

with a real diffusion coefficient $|a|^{-1}$. The simpler complex Ginzburg-Landau equation (43) is able to catch the main qualitative features of the system behavior. The dynamics of (43) is known [79, 91, 92] to possess various phase transitions, spiral defects (e.g. for $d = -0.75 + i$), and defect turbulence (e.g. for $d = -0.1 + i$); these phenomena can be observed also in the delay equation for the variable $z(t)$. This will be discussed in more detail in Sec. 6.8.

4.5 Open questions for normal forms

The above destabilization theory for long-delay systems takes in account two basic points: The description of the spectrum determining the main (co-dimension 1) destabilizations, such as uniform, wave, and modulational. The second, the derivation of normal forms which describe the dynamics within the class of systems, that are undergoing a particular destabilization transition.

However, there are still open questions, such as

- The uniform destabilization is treated for a general class of *scalar* DDSs (Sec. 4.2), thus the vector case represents an open problem in general. The case of wave destabilization has been considered so far for two paradigmatic examples (1D and 2D case) only, see Secs. 4.3 and 4.4. The normal forms for the general vector case DDS $x'(t) = f(x(t), x(t-\tau))$ are still to be derived.
- Determination of the normal form for the modulational instability.

4.6 Interpretation of delay-equation as a hyperbolic PDE

The delay-equation (1) can be equivalently interpreted as a hyperbolic PDE by introducing the function of two variables $u(\theta, t)$ as

$$u(\theta, t) = x_t(\theta) = x(t + \theta). \tag{44}$$

Equation (1) can then be written as the following transport system, where the nontrivial dynamics is introduced mainly by the boundary condition

$$\begin{cases} \frac{\partial u}{\partial t}(\theta, t) - \frac{\partial u}{\partial \theta}(\theta, t) = 0, & \theta \in [-\tau, 0),\ t \geq 0 \\ \frac{\partial u}{\partial \theta}(0, t) = F(u(0, t), u(-\tau, t)), & t \geq 0 \quad \text{(boundary cond.)} \\ u(\theta, 0) = \varphi(\theta), & \theta \in [-\tau, 0] \quad \text{(initial cond.)}. \end{cases} \tag{45}$$

The first equation follows from the definition (44), the second one from (1) by noting that $x(t) = u(0, t)$, and the third one is the initial condition. Such a procedure, in contrast to the reduction to the parabolic PDE discussed in the previous sections 4.1–4.4, does not simplify the problem, and just provides an equivalent representation. From the point of view of the PDE theory, Eq. (45) is a hyperbolic initial boundary-value PDE problem, which is especially challenging since the boundary condition contains a nonlinearity and a derivative.

5 The physical meaning of the long-delay limit

Long-delay systems manifest most of their peculiar features already in the phenomenology shown by the time series. Numerical simulations of complex models as well as data from complicated experimental setups can quickly reveal, when re-organized and analyzed with a suitable representation the basics elements for the presence of an equivalent space-time dynamics. While a quantitative description can only be drawn in terms of specific indicators and in the asymptotic regimes, preliminary indications often requires only a careful inspection of the reorganized patterns.

In this section, we discuss the physical meaning of the indicators for the space-time dynamics in long-delay systems.

5.1 Information propagation and causality

As discussed in Sec. 2, the spatio-temporal representation is, in fact, a re-organization of the temporal series. As long as the spatial size chosen is equal to the delay time (or

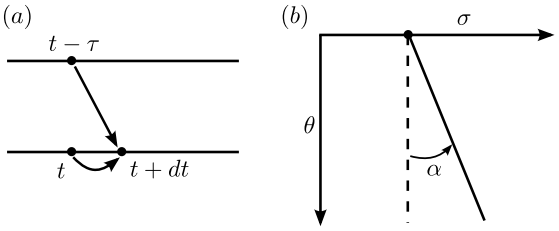

Figure 11: (a) STR coupling; (b) Comoving angle for the maximal comoving Lyapunov exponent.

sometimes multiple delay times), the propagation of structures in the pattern is clearly characterized by a *drift*, as illustrated in Fig. 1. While it can be quantified by the analysis of the autocorrelation function and derived from more fundamental, microscopic quantities, its existence can be understood using the following simple considerations. In a DDS, the time evolution is governed by a *local* (i.e., at time t) derivative expressed in terms of the *local* and *past* (i.e., at time $t-\tau$) terms. When represented in the STR (see Fig. 11), it is apparent that the past term cannot influence the dynamics before (or even at) the time t. In other words, there should exist a space-time bound for the world lines originating in the past (events cone).

The previous considerations can be precised by the analysis of the propagation of the space-time disturbances, as described by the *maximal comoving Lyapunov exponent* (MCLE) [93, 94, 75, 95]. Generally speaking, the MCLE can be defined as the rate of divergence (or convergence) of small *localized* perturbations of trajectories in an extended system, as a function of a suitable comoving angle α (see Fig. 11(b)). At variance with the standard Lyapunov analysis, which is effective for absolute instabilities only, the MCLE can be used for studying convective instabilities [96] as well.

In DDS, it has been shown [75] that using the STR the MCLE can be defined as in spatially extended systems and its analytical expression can be derived for the linear model (19), obtaining

$$\Lambda(\alpha) = a \sin\alpha + (1 + \ln(|b| \tan\alpha) \cos\alpha. \tag{46}$$

From the above expression, we notice the following features:

- The MCLE is a function of the comoving angle α, representing the inclination of *world*-lines starting at a fixed point σ within the pseudo-space (origin of the disturbance) and increasing along the pseudo-time θ (Fig. 11). Such a function displays a maximum at a fixed angle α_0 corresponding to the above-mentioned *drift*.

- In the case $\alpha \to \pi/2$, the MCLE approaches the coefficient of the local term. In such a case, it is negative for an effective STR but it may become positive as well, thus corresponding to the *anomalous (strongly unstable)* Lyapunov exponent [38] and to the settling of the *strong* chaos regime [65].

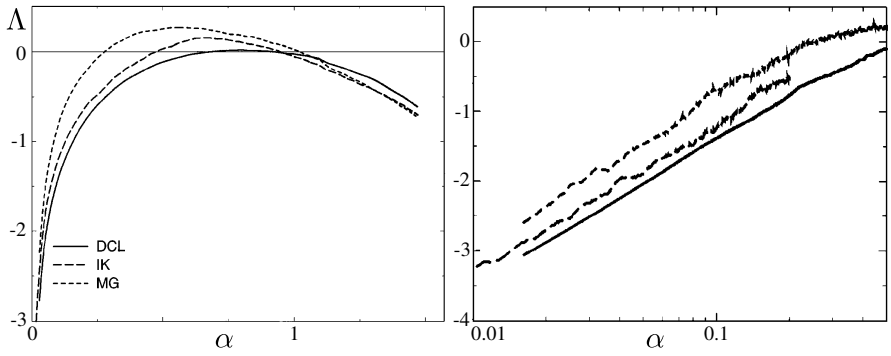

Figure 12: Comoving Lyapunov spectra for the delayed complex Landau model, Ikeda model, and Mackey-Glass equation (left). Logarithmic tails are reported in the right figure. (The figure is adapted with permission from Ref. [75]. Copyrighted by the American Physical Society.)

- The MCLE is not defined for $\alpha < 0$ and it asymptotically diverges when $\alpha \to 0^+$, indicating the bound of the events cone for the information propagation. The tail at $\alpha = 0^+$ displays a logarithmic behavior (see Fig. 12).

The bound at $\alpha = 0$ is the expression of *causality*: the system at a given (pseudo) space position can receive information from the (pseudo) past only from the leftmost spatial positions. Otherwise, a propagation faster than the evolution speed would be required, i.e. an ability to travel one delay unit in a time shorter than τ.

The dependence of the MCLE on the propagation angle is similar for different models, as numerically shown in Fig. 12. Notably the asymptotics at the causality bound is always logarithmic; this is related to the finite response time of the system, which is unable to respond instantaneously at a delayed stimulus.

In general and in presence of *weak* chaos (see Sec. 6.4) it is expected that the main features of the MCLE remain the same. An example is presented in Fig. 13, where the MCLE is calculated from an experimental time series obtained in a a CO_2 laser setup [43] using a model-reconstruction technique especially developed for delay systems [98]. In this example, the horizontal and vertical arrows superimposed to the STR of the data indicate the directions corresponding to the zeros of the MCLE (plotted in the inset). The comoving function is evaluated by the linearized maps obtained from the reconstruction method, as a direct result from the experimental data. In the paper, it is argued that the MCLE zeros correspond to macroscopically observable propagation of structures, since the disturbances neither diverges nor shrink exponentially along such directions. As a consequence, they should correspond to the leading contributions to the bidimensional autocorrelation function of the data. While this is actually the case in examples of spatially extended systems, in the delayed case only one (the smaller) of the two velocities corresponds to that found from the correlation analysis.

A generalization to the case of multiple, hierarchically long delays has been recently presented and discussed in [49]. In the case of two delays, the propagation of struc-

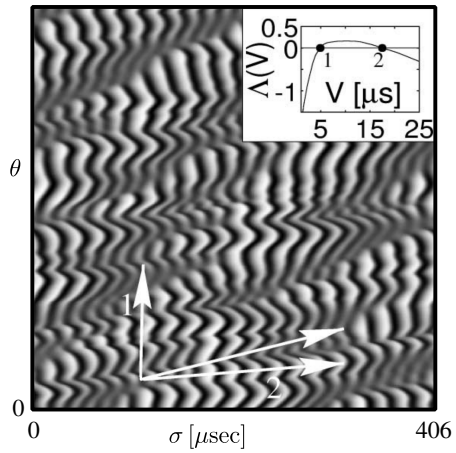

Figure 13: Space-time representation of the field intensity in the CO_2 laser experiment. The horizontal space-like variable denotes the position within one delay window, while the vertical time-like variable labels the windows. The central arrow denotes the direction characterized by the maximal growth rate. Inset: the maximal comoving Lyapunov exponent. (The figure is adapted with permission from Ref. [97]. Copyrighted by the American Physical Society.)

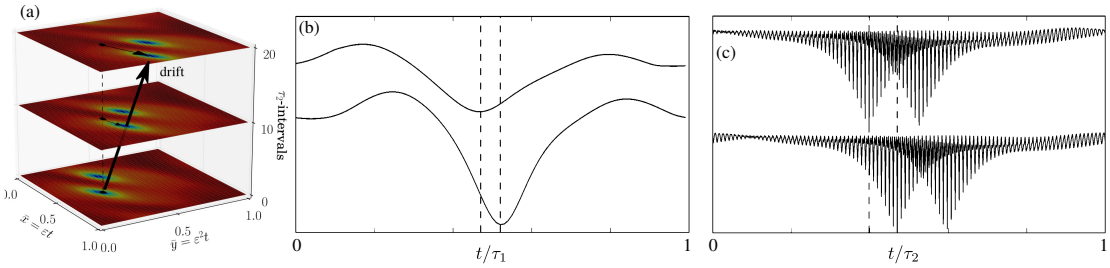

Figure 14: (color online) Drift in the propagation of defect structures in a two-delays system. Using the STR with the uncorrected pseudo-space variables the defects are moving in the pseudo-time (a). The components of the (vectorial) drift can be evidenced by plotting two successive, 2-long (b) and 1-long slices (c). The separations between the two vertical dashed lines are y (b) and x (c) drift components respectively. (The figure is adapted with permission from Ref. [84]. Copyrighted by the American Physical Society.)

tures is illustrated showing the (vectorial) drift in a two-dimensional STR (see Fig. 14). Introducing a spherical coordinates system (ρ, α, β) such that the variables of the STR

$$t = \sigma + n\tau_1 + m\tau_2$$

can be written as $m = \rho\cos\alpha$, $n = \rho\sin\alpha\cos\beta$, $\sigma = \rho\sin\alpha\sin\beta$, it is found that the MCLE of the linear system

$$\dot{z}(t) = az(t) + bz(t-\tau_1) + cz(t-\tau_2)$$

can be calculated explicitly, yielding

$$\begin{aligned} \Lambda(\alpha,\beta) &= a\sin\alpha\sin\beta + (1+\ln(|b|\tan\beta))\sin\alpha\cos\beta + \\ &\quad +(1+\ln(|c|\sin\beta\tan\alpha)\cos\alpha. \end{aligned} \tag{47}$$

If is apparent that expression (47) is a two-dimensional generalization of (46).

The arrow in Fig. 14 follows the direction defined by the maximum of $\Lambda(\alpha,\beta)$. We remark that, since for an arbitrary parameters choice the angles are generically nonzero and bounded below by $\pi/2$, the disturbances always propagate with a drift. We notice how the comoving exponent diverges logarithmically close to the axis $\alpha = 0$ and $\beta = 0$, i.e. instantaneous propagations are forbidden. In the opposite limit, $\alpha \to \pi/2$ (resp. $\beta \to \pi/2$), it approaches the value for the single delay case $c = 0$ ($b = 0$). Finally when both $\alpha, \beta \to \pi/2$ (infinite velocity), $\Lambda = a$ and the dynamics is governed by the local term as expected.

5.2 Multiple timescales and the continuum approximation

The STR is based on the splitting of the time t in two variables, the continuous, space-like σ within a delay and the integer, time-like θ indexing successive delay units; they correspond to well-separated time scales. In such a representation, the dynamics if often similar to that of 1-D, spatially extended system as discussed above: the pattern obtained may show correlations, both in space and time on possibly long ranges, resulting in a clear and well defined two-dimensional structure.

The general context for such a picture, as discussed in Sec. 4 is the multiple timescales analysis. Whenever a smooth two-dimensional pattern can be obtained from the representation, there should exist a mapping to a spatially-extended model generating the same pattern. More precisely, the delay system generates a *sampled* sub-pattern, with integers in the time-like variable, embedded in the pattern generated by the equivalent spatial model.

The existence of such a mapping is at the basis of the *continuum approximation*, i.e. the delay pattern appears smooth: the difference between successive, corresponding spatial points is small, as the scale for the relevant variations is much larger in the time-like variable. Conversely, in the case of strong chaos such approximation fails, as the local instability along the space-like variable (anomalous or strongly unstable Lyapunov

exponent) strongly decorrelates successive elements in the STR. It should be noted, however, that the strong chaos is defined in a statistical sense: even if asymptotically the anomalous exponent exists, it could be possible to build a meaningful STR for short times, where dynamical fluctuations might set a local, weak-chaos-like regime.

5.3 The form of boundary conditions

The formal approach for the definition and use of the multiple timescales including boundary conditions has been discussed in Sec. 4. Here we discuss the form of the bounday conditions in view of the representation described by Eq. (3). It holds

$$t = \sigma + \theta\tau = (\sigma + \tau) + (\theta - 1)\tau$$

leading to the connection between the values of the solution that are separated by τ along the pseudo-spatial variable and by 1 along the pseudo-temporal one:

$$y(\sigma + \tau, \theta - 1) = y(\sigma, \theta).$$

By assuming that the solution is slowly changing along the pseudo-temporal variable $y(\sigma + \tau, \theta - 1) \approx y(\sigma + \tau, \theta)$ (e.g. by strong correlation), and rescaling the spatial variable by τ, we eventually find the periodic boundary conditions:

$$y(x, \theta) \approx y(0, \theta), \tag{48}$$

besides the appearance of a drift as noted before.

In the case of multiple delays, treated in Sec.4, boundary conditions are more complicated reflecting the interplay of the different timescales; however, the physical background and the way the systems approaches the thermodynamic limit is very much the same.

5.4 Multiple delays and spatio-temporal representation

The spatio-temporal representation can be used as well when the system contains an arbitrary number of delays, in the case their magnitudes are ordered hierarchically [84]. Consider a dynamical system with a natural timescale t_0, with N feedback loops each with a time lag τ_k $(k = 1, ..., N)$. We assume that, introducing the smallness parameter $\epsilon = t_0/\tau_1 \ll 1$ the delays can be written as $\tau_k = t_0\epsilon^{-k}$. A natural choice for the multiple scales is now $T_l = \epsilon^l t$, l being a positive integer number.

In this case, we expect that $\{T_l,\, l = 1, .., N\}$ represent the *"spatial"* scales. The T_{N+1} is now the scale of the "*drift*", as measured e.g. microscopically with the help of the comoving Lyapunov exponent or with the autocorrelation function [97]. The expected scale for the equivalent normal form dynamics is T_{N+2}.

In general case, we can define the STR (Eq. 3), with the variables σ_0, n_j, and Θ defined by

$$\begin{aligned}
[t/\tau_N] &= \Theta \\
[(t-\Theta\tau_N)/\tau_{N-1}] &= n_{N-1}, \\
[(t-\Theta\tau_N - n_{N-1}\tau_{N-1})/\tau_{N-2}] &= n_{N-2}, \\
&\ldots \\
[(t-\Theta\tau_N - n_{N-1}\tau_{N-1} - \ldots - n_2\tau_2)/\tau_1] &= n_1, \\
t-\Theta\tau_N - n_{N-1}\tau_{N-1} - \ldots - n_1\tau_1 &= \sigma_0.
\end{aligned}$$

It holds that $\sigma_0 \in [0, \tau_1]$. Because the pseudo-spatial variables n_k can assume large values and are bounded by $[\tau_{k+1}/\tau_k]$, we use the rescaled *pseudo-spatial* variables $S_0 = \sigma_0/(\tau_1/t_0)$ and $S_k = n_k/(\tau_{k+1}/\tau_k)$, $k = 1, \ldots N-1$, which are restricted to the interval $[0, 1]$, and the *pseudo-temporal* variable $T = \Theta/(t/\tau_N)$. We obtain

$$\begin{aligned}
\sigma_0/t_0 = \sigma_0/\tau_1 \cdot \tau_1/t_0 &= S_0\varepsilon^{-1}, \\
n_1\tau_1/t_0 = n_1/(\tau_2/\tau_1)\cdot(\tau_2/\tau_1)\cdot(\tau_1/t_0) &= S_1\varepsilon^{-2}, \\
&\ldots \\
n_{N-1}\tau_{N-1}/t_0 = n_{N-1}/(\tau_N/\tau_{N-1})\cdot\ldots(\tau_1/t_0) &= S_{N-1}\varepsilon^{-N} \\
\Theta\tau_N/t_0 = \Theta/(t/\tau_N)\cdot(t/t_0) &= T\varepsilon^{-(N+1)},
\end{aligned}$$

The STR can be written now as

$$\bar{t} = t/t_0 = S_0\varepsilon^{-1} + S_1\varepsilon^{-2} + .. + S_{N-1}\varepsilon^{-N} + T\varepsilon^{-(N+1)}. \tag{49}$$

It is now easy to recognize how the STR can be related to a multiscale analysis: the dynamics on the timescale $T_l = \varepsilon^l t$ is visible on the coordinate l only, since the scales $k < l$ are too fast and the $k > l$ too slow.

The drift (acting on the scale T_{N+1}) and the possible effective normal form dynamics (evolving in the comoving reference frame, with scales equal or longer than T_{N+2}), can be visualized with the help of the STR in the pseudo-time range $t/\tau_N \simeq \varepsilon^{-1}$ and $t/\tau_N \simeq \varepsilon^{-2}$ respectively.

The above approach is a formal framework and represents an interpretation of the STR that can be built in such a case; however, a rigorous derivation of the normal forms or even the interpretation of the interplay between the different time scales will have to be discussed case by case.

6 Spatio-temporal phenomena in the theory of delay systems

The choice of a suitable representation, as discussed in the previous sections, allows to map purely temporal behavior to spatio-temporal phenomena. In this section, numer-

ical[3] and analytical examples of this approach are presented in the context of different models and regimes, showing its effectiveness in disclosing the features of the dynamics hidden behind such complex temporal behaviors.

6.1 Spatio-temporal chaos in 1D

A first evidence of spatio-temporal chaos induced by long delay feedback was reported in [75, 45] for a Stuart-Landau oscillator with delayed feedback

$$\frac{dz}{dt}(t) = \mu z(t) - (1+i\beta)z(t)|z(t)|^2 + \eta z(t-\tau). \tag{50}$$

The spatio-temporal chaos was shown for $\mu = -0.8$, $\eta = 1$, and $\beta = 3$, in the vicinity of the destabilization $\mu \approx -\eta$. In such a regime, the amplitude equation (see Sec. 4.3) of the form

$$\eta \partial_\theta A = \mu_1 A + \frac{1}{2\eta}\partial_{xx} A - (1+i\beta)A|A|^2$$

was derived, where $\mu_1 = (\mu+\eta)\tau^2$. Due to the nonzero imaginary part of the nonlinearity $\beta \neq 0$, the obtained normal form exhibits spatio-temporal chaos, which is qualitatively similar to that observed in (50) for the corresponding parameter values.

6.2 Eckhaus instability

This section summarizes the results presented in [46], showing the existence of the Eckhaus destabilization in delay systems. The Eckhaus phenomenon was first reported in [103], where a general framework was proposed for studying the stability of periodic patterns in Ginzburg-Landau equation, and, in particular the dependence of their stability on the wavelength. The classic Eckhaus instability diagram for a PDE on infinite domain is shown in Fig. 15(a), where q_a is the wavenumber of a periodic pattern ($e^{iq_a x}$ for GLE) and α is the destabilization parameter. Increasing α, periodic patterns with wavenumber q_a appear at the line H and become asymptotically stable at the Eckhaus line E. After the destabilization of the homogeneous state, there appear many stable periodic waves (infinitely for infinite domain, and finitely many for a bounded domain [104]).

In [46], it is shown that the delay system

$$\frac{dz}{dt}(t) = (\alpha+i\beta)z(t) - z(t)|z(t)|^2 + z(t-\tau) \tag{51}$$

[3] *A note on numerical methods:* The numerical integration of delay systems with fixed delays usually employs the standard methods existing for ODEs such as Runge-Kutta, etc. The algorithms should take care of of the saved history from the previous (maximal) delay interval to manage the integration steps. One of such methods is e.g., pydelay package for python [99]. In order to resolve the fast transitions layers, more advanced algorithms can be adopted, e.g., in [100, 101] the authors used an algorithm of recurrent Taylor expansion of the 30th order with a constant time step. To numerically exploit bifurcation diagrams, the package DDE-Biftool is widely applied [102]. The above utility allows also the determination of the spectrum of eigenvalues and Floquet multipliers.

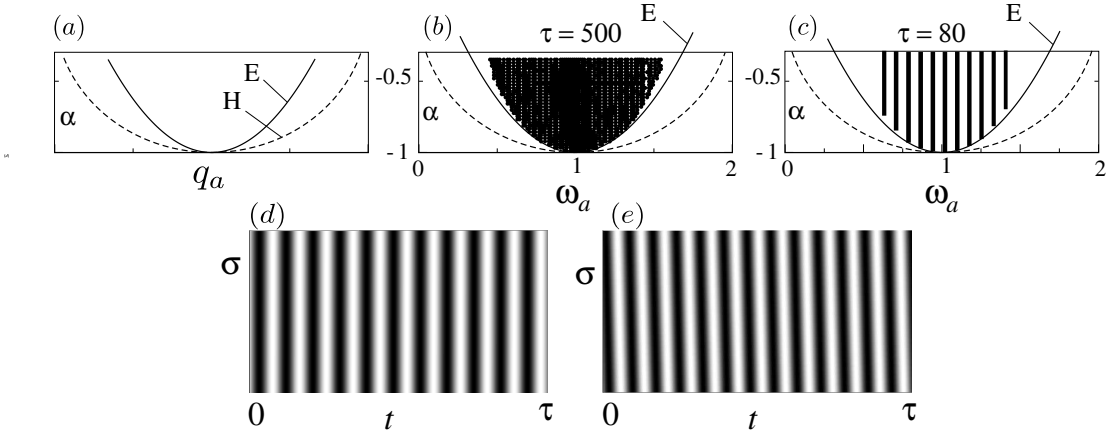

Figure 15: Eckhaus instability in delay system (51). (a) Classic Eckhaus instability diagram. q_a is the wavenumber and α is the destabilization parameter. Line H marks where periodic waves with wavenumber $q_a$appear and E is the Eckhaus line where these patterns become unstable. (b) and (c) are the corresponding bifurcation diagrams for the delay system (51), where the frequency ω_a of periodic solutions plays the role of the wavenumber. Figures (d) and (e) show the spatio-temporal representation of the related periodic solutions; the difference is in the number of peaks (wavenumber).

is close to the wave destabilization for $\alpha \approx -1$ (see also Sec. 4.3), and its normal form is the Ginzburg-Landau equation (37) where the Eckhaus destabilization takes place. A corresponding Eckhaus phenomenon is thus present in DDS (51), and multiple stable periodic solutions are found after the destabilization point (for α values larger than $\alpha = -1$). The number of coexisting stable periodic solutions is shown to be proportional to the delay τ, hence, the time delay plays a role similar to the size of the spatial domain (see Fig. 15).

We remark that the main difference between the system (51) and (50) is the value of the imaginary part of the nonlinearity, which is $\beta \neq 0$ in (50).

6.3 Stripes and square waves

A remarkable topic in systems with large delays is the existence of square wave solutions. Their origin has been thoughtfully investigated theoretically [24, 105, 106, 107, 5, 53]. In their simplest form, they are shown in Fig. 16(d) where plateaus of approximately constant lengths close to τ are connected by sharp fronts. In fact. the period of such a solution is $2(\tau + \delta)$, where δ accounts for the drift (see Sec. 4). Higher harmonics could also be observed, where the plateaus are shorter [106]. The bifurcation mechanism behind the appearance of the multiple coexisting square wave oscillations resembles the Eckhaus phenomena discussed in Sec. 6.2. Systems, which possess periodic square waves, usually exhibit also solutions with irregular alternating plateaus [Fig. 16(c)], which are also "almost" 2τ periodic, but in fact they are very long transients.

A spatio-temporal representation of such solutions can be made using the space

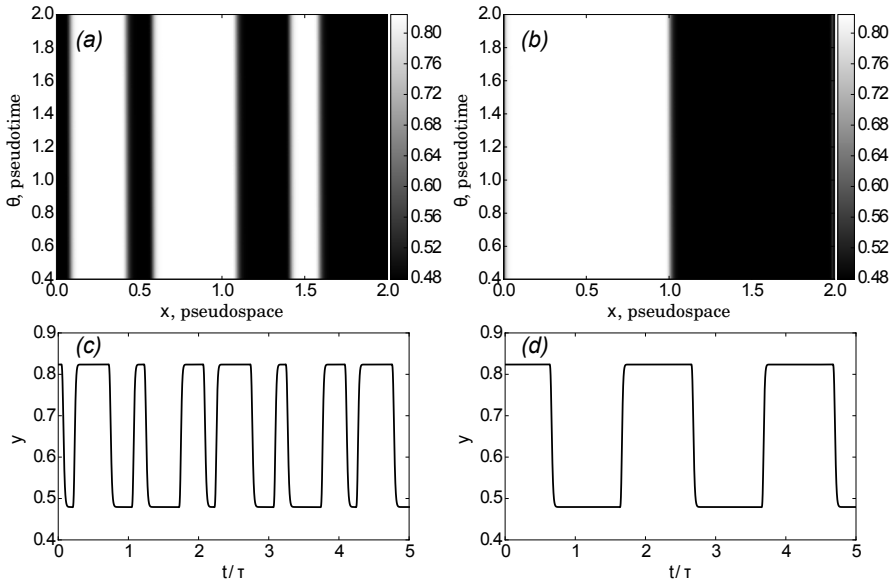

Figure 16: Square wave solutions (bottom row) of system (52)–(54) and their spatio-temporal representation (upper row). The corresponding reduced map (54) has a stable period-2 solution that determines the plateaus of the square-wave solution. Note that the pseudo-spatial interval of the length $\approx 2\tau$ (two consecutive delays) is used for the spatio-temporal representation, since $y(t+\tau+\delta) \approx -y(\tau)$. The drift δ has been taken into account obtaining a vertical stripes pattern.

interval of the length $2(\tau+\delta)$ instead of $\tau+\delta$; the spatio-temporal patterns associated to the square waves are stripes as shown in Figs. 16(a) and (b). The square waves are thus represented by an even set of ascending and descending fronts. The dynamics of these fronts was to some extent investigated in [53] as well as in [106].

In order to explain the origin of the square wave oscillations, let us consider the scalar DDS

$$y'(t) = -y(t) + f(y(t-\tau)). \tag{52}$$

By rescaling the time $t \to t/\tau$, we obtain

$$\frac{1}{\tau} y'(t) = -y(t) + f(y(t-1)).$$

By formally setting the left-hand side to zero for $1/\tau \to 0$, one obtains the discrete map

$$y(t) = f(y(t-1)), \tag{53}$$

where, however, t is still the (continuous) time. Now, let us consider the case when the map (53) has a stable period-2 solution such that $y_2 = f(y_1) = f(f(y_2))$ with some fixed y_1 and y_2. In such a case, starting from an initial condition, the map (53) will converge to the solution alternating between y_1 and y_2. In particular, the solutions of the form shown in Figs. 16(c) and (d) appear with exact period 2τ and infinitely steep fronts

between them. As we have seen from the asymptotic analysis in Sec. 4, the neglected term $\frac{1}{\tau}y'(t)$ adds a diffusion effect and a drift. As a consequence, among all possible solutions of the map (53), only those survive that have a more smooth profile within the intervals of almost constant plateaus. Additionally, a drift δ appears as well.

Numerical examples in Fig. 16 are presented for the system (52) and for the case

$$f(y) = \mu y(1-y), \tag{54}$$

corresponding to the logistic map. The parameter $\mu = 3.3$ is chosen such that the map has a stable period-two solution.

It is instructive to emphasize the form of the normal form equations for the DDS (52) close to the period-doubling bifurcation of the reduced map (53); there, it holds $f'(y) = -1$, and the situation is exactly as considered in Sec. 4.2. Hence, the normal form equation close to such an instability has the form (32) with the anti-periodic boundary condition $A(x,\theta) = -A(x-1,\theta)$. Such a boundary condition corresponds to the flip of the solution from y_1 to y_2 (or vice-versa) after the time interval $\tau + \delta$.

The above-mentioned period-doubling bifurcation of the reduced map leads also to an interesting effect for the spectrum of the steady state close to the destabilization [49]. It corresponds to the uniform destabilization, see Fig. 7 with the leading eigenvalues of the form $\lambda_k = i\frac{1}{\tau}(\pi + 2\pi k) + \mathcal{O}(\frac{1}{\tau^2})$, $k = 0, \pm 1, \pm 2, \ldots$. Such a form of the spectrum explains the emergence of the 2τ-periodic solution at the destabilization of the steady state as well as the other subharmonic bifurcations.

Similar situation occurs when the reduced map possesses a periodic solution with a higher period n. In such a case, the spatio-temporal representation should involve the intervals of a length $n(\tau + \delta)$.

We conclude this section with the following remarks:
– Stable asymmetric square waves of a period close to *one* delay are possible as shown in [108], however, they are found not in a scalar delay system, but in a system with two variables, similarly to the system where chimera states are observed, see Sec. 7.5.
– In [109], a comparison of the discrete reduced map (53) with the original delay system (52) is discussed and experimentally investigated in an optoelectronic setup. In particular, a period-three window in the chaotic regime is observed corresponding to the window for the map.
– By introducing a second delay, the amplitude of the square waves can be modulated in a nontrivial way, as discussed in [110].

6.4 Strong and weak chaos

In Sec. 3 we have discussed how the Lyapunov exponents of systems with long time delayed feedback can scale generically as $1/\tau$ or as $\mathcal{O}(1)$, i.e. do not scale with τ. In the latter case, if such a Lyapunov exponent is positive, it can be estimated from the truncated ODE (22), where the Jacobi matrix $A(t)$ is evaluated on the solution $s(t)$ of the full delay system $A(t) = \partial_1 F(s(t), s(t-\tau))$. The number of such strongly unstable Lyapunov exponents is limited by the number of components of $x(t)$.

When the dynamics has strongly unstable Lyapunov exponents, the regime can be called *strong chaos*. Indeed, in such a case the perturbations grow exponentially on time intervals $1/\lambda_{\max}$ that are much smaller than the delay τ, i.e. the sensitive dependence on initial conditions reveals on scales much shorter than τ.

On the other hand, in many situations strongly unstable Lyapunov exponents are absent. For instance, this happens in the Mackey-Glass [1] system

$$\frac{dx(t)}{dt} = -\gamma x(t) + \beta \frac{x(t-\tau)}{1+x^n(t-\tau)}, \ \gamma > 0,$$

for which $A(t) = -\gamma$ is constant and negative, and, hence, the truncated ODE $x'(t) = -\gamma x(t)$ cannot have a positive LE. In such a situation, chaotic attractors possess families of positive Lyapunov exponents that scale as $1/\tau$. Such a situation is called *weak chaos*.

Examples for the Lyapunov exponents in the strong and weak chaos regime are shown in Fig. 17 for the Lang-Kobayashi model

$$\begin{aligned} E'(t) &= (1+i\alpha)N(t)E(t) + \eta E(t-\tau), \\ N'(t) &= \varepsilon \left[J - N(t) - (2N(t)+1)|E(t)|^2 \right], \end{aligned} \tag{55}$$

where $E(t)$ is the complex field amplitude and the real variable $N(t)$ the carrier density. This system displays both regimes depending on the parameters. In particular, by changing the pump current parameter J, the initially stable "off-state" $E = 0$ destabilizes and, if the time delay is large enough, increasing J the system quickly reaches a weakly-chaotic state that is characterized by the family of positive LEs scaling as $1/\tau$. The dependence of LE's on time delay is shown in Fig. 17(b,d). The LEs approach a continuous spectrum when $\lambda_j(\tau)\tau$ is plotted versus j/τ where j is the number of LE accordingly to its magnitude, see Fig. 17(c). When the pump current J is further increased, the strong chaos appears, characterized by a positive maximal Lyapunov exponent that does not scale with τ, see Fig. 17(a).

An useful approach for estimating the scaling of LEs in the transition between the strong and weak chaos is the stochastic modeling [35, 72]. In particular, in [72] a linear stochastic model for the dynamics of a perturbation for a delay system is proposed, which has a multiplicative noise in its instantaneous part. Such a model contributes to the explaination of the scaling laws of LEs.

More details about strong and weak chaos can be found in [38, 65].

6.5 Coarsening

Spatiotemporal dynamics in bistable media is often characterized by the appearance of fronts that are bounding domains with different homogeneous states (phases). For example, fronts appear in reaction-diffusion equations, where local bistable dynamics couples to the spatial degrees of freedom via a diffusion term. A simplest example is given by a one-component system [111]. When such a system is prepared in an inhomogeneous initial state, the resulting typical patterns are formed by domains of homogeneous states separated by moving fronts: they propagate without changing their

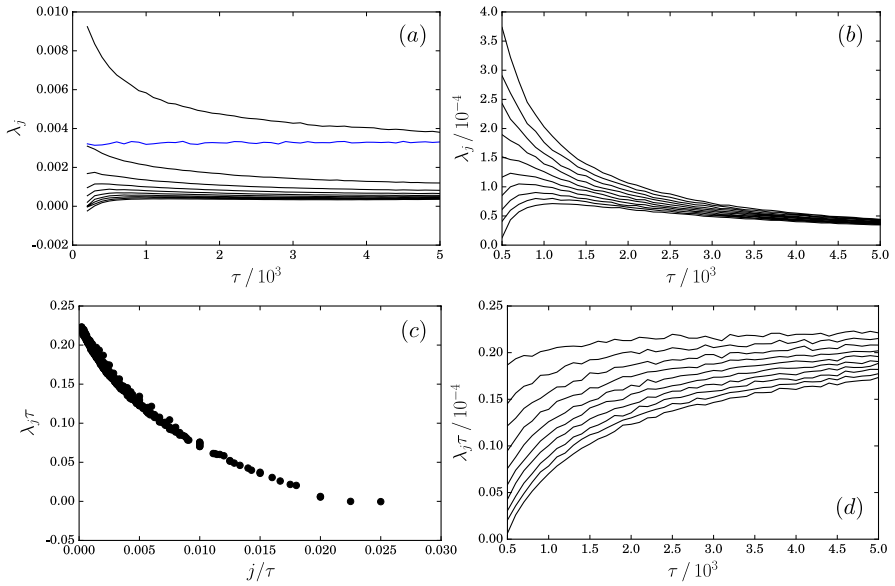

Figure 17: Lyapunov exponents for the Lang-Kobayashi system (55) versus time delay τ. (a) Strong chaos for $J = 0.075$; (b-d) weak chaos for $J = -0.05$. Other parameters: $\varepsilon = 0.03$, $\eta = 0.1$, $\alpha = 5.0$, and $\varphi = 0.5$.

shape and annihilate in pairs. This process eventually leads to a globally homogeneous landscape, a process known as *coarsening* [112]. Which of the two phases will eventually fill the whole space, as well as the propagation speed of the fronts would depend on the shape of the corresponding double-well potential.

In [100], the coarsening phenomena is shown to take place in the bistable systems with long time delayed feedback

$$\frac{dx(t)}{dt} = -U'(x(t)) + gx(t-\tau), \tag{56}$$

where $U(x)$ is a double-well potential with $U'(x) = x(x+1+a)(x-1)$. For $a = 0$ the potential is symmetric and the value of a measures the asymmetry of U. The parameter g determines the strength of the delayed feedback. In the absence of the feedback, this system is bistable, i.e. depending on the initial conditions it approaches one of the two stable steady states. With nonzero feedback, the steady states are modified as $x_\pm = (-a \pm \sqrt{(2+a)^2 + 4g})/2$, and they remain stable in some range of the parameter g. As a result, for initial conditions $\varphi(s)$ $(-\tau \le s \le 0)$ that are close to one of these steady states, the solution will eventually converge to it. However, when the system is not close initially to either x_- or x_+, the solution displays oscillations which rapidly acquire the nearly rectangular form of alternating plateaus close to the steady states (phases) $x_\pm$, separated by ascending and descending fronts. In the course of time, one of the phases gradually expands at the cost of the other, until the steady solution gets eventually established. The "winning" solution is determined by the asymmetry a of the potential. The largeness of the time delay τ in this case is necessary for the existence of

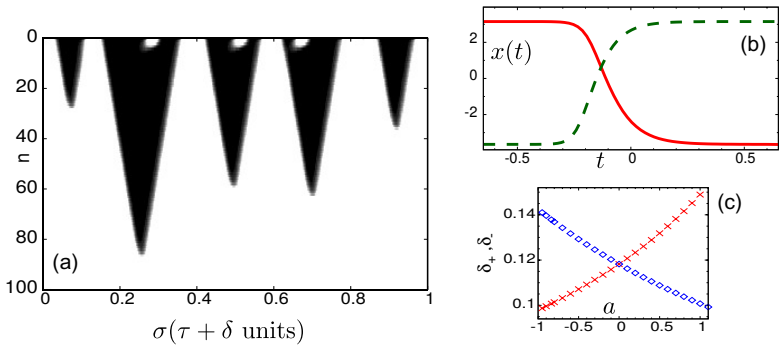

Figure 18: (Color on-line) (a) Motion of fronts and coarsening in Eq. (56) at $a = 1.5$, $g = 1$, and $\tau = 10$. (c) Homo- and heteroclinic states in Eq. (57) at $a = 0.5$, $g = 10$. Solid line: descending front with the velocity $\delta_- = 0.13183$. Dashed line: ascending front, $\delta_+ = 0.10882$. (d) Front velocities at $g = 10$, computed from Eq. (57). Crosses: descending fronts; diamonds: ascending fronts.

at least several stationary phases and the switching episodes between them within one delay interval.

A proper interpretation of the phenomenon described above is obtained using the spatio-temporal representation as described in Sec. 2.1. A typical spatio-temporal plot for the positive feedback is shown in Fig. 18(a), where the coarsening of the phases can be clearly observed. For the given parameter values, the white color corresponds to the phase with x_+, and this phase "wins" because of the asymmetry of the double-well potential. The velocities and the shapes of the fronts are shown in Figs. 18(b-c). The so called Maxwell point at $a = 0$ is also observed, where the velocities of the ascending and the descending fronts coincide. In [100] it is shown that the "profile equation" determining the velocity δ and the shape of the front is given by the system with advanced argument

$$\frac{dy(t)}{dt} = -U'(y(t)) + gy(t+\delta). \tag{57}$$

The fronts are given as heteroclinic solutions of this equations, and the velocity δ is determined from the condition that such a heteroclinic solution exists. Further analytical results (e.g. scaling of the coarsening time) are possible to obtain by applying post-newtonian approximation to (57) assuming that the velocity δ is small, see [100].

6.6 Nucleation

The term *nucleation* refers usually to a spatial effect in the context of phase transitions of the first order: the birth of localized buds of the new phase in the bulk of the old one. Typically, when the nucleus of the new phase is created inside the old one, the gain in free energy is proportional to the nucleus volume whereas the loss is proportional to its surface area. The balance is reached at a certain critical size of the nucleus, below which

the nuclei shrink [113]. In the context of reaction-diffusion systems, nucleation occurs in bistable situations, in which one of two stable regimes dominates. Here, again, survival and subsequent growth of the newborn nucleus of the dominating phase require that at the moment of birth this nucleus occupies a sufficiently large portion of available space [114, 115]. In one-dimensional, spatially extended systems nucleation has been studied in e.g. amplitude equations [92] or in excitable media [116].

In [101] the evidence of one-dimensional nucleation has been given which, in a seeming contrast to the above cases, occurs not in space but in time. Accordingly, a nucleus occupies not the spatial region but a time interval, and the critical size is replaced by a critical duration. This effect takes place in bistable, long-delayed dynamical systems. In particular, the model as well as the corresponding spatio-temporal representation is the same as in the previous Sec. 6.5, and is given by Eq. (56). Figures 19(a) and (b) illustrate how a small nucleus of the "winning" phase shrinks because of its initial size is not large enough.

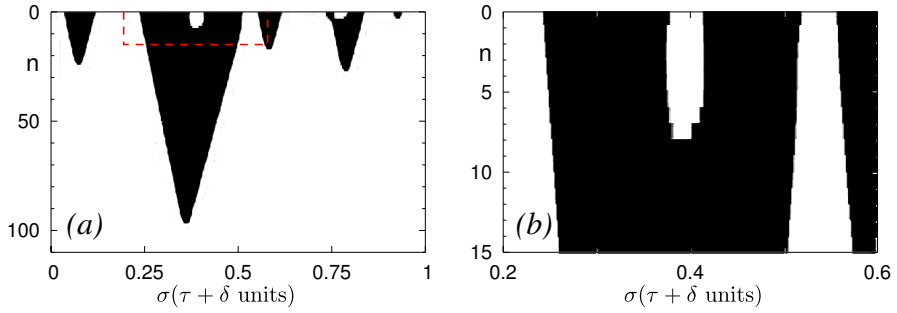

Figure 19: Coarsening and nucleation in pseudo-space of Eq. (56). In the zoom in Fig. (b), there is a small nucleus of the white phase, too small to determine the expansion of its phase, even though this phase is preferred by the choice of the bistable potential (see more details in [101]).

By gradually increasing the width of the nucleus, one can find the critical nucleus which theoretically exists and is stationary for an infinitely large time. Dynamically, the critical nucleus can be viewed as an unstable periodic solution of Eq.(56) with period $\tau + \delta$ and a single Floquet multiplier outside the unit circle. The stable manifold of this solution has codimension 1 and serves in the phase space as part of the boundary between the attraction basins of two fixed points which correspond to the strong and the weak phases, respectively.

We should remark that for positive values of the delay feedback g the equation (56) is a monotone dynamical system and, hence, cannot possess stable periodic solutions [117]. However, in the case of vanishing asymmetry $a = 0$, the relevant periodic state can be made nearly neutrally stable, that prolongs noticeably the life of slightly subcritical nuclei.

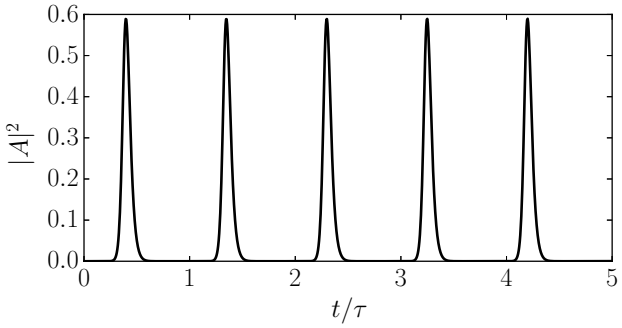

Figure 20: Periodic solution of the model for mode-locked laser (58) for parameter values $\gamma = 33.3$, $\kappa = 0.1$, $\alpha_g = 0$, $\alpha_q = 0$, $\psi = 0$, $G_0 = 0.6$, $Q_0 = 1.2$, $\gamma_g = 0.0133$, $\gamma_q = 1$, $s = 25$, and $\tau = 2.0$. The solution has the form of narrow pulses with the period close to the time delay τ.

6.7 Pulses and localized structures

One relevant example of localized solutions existing in the pseudo-space of systems with time delay is found in delay-models for mode-locked lasers [118, 119]. More specifically in [118] the mathematical model for a ring laser with a saturable absorber is derived in the form of delay-differential equation as

$$\begin{aligned} \dot{A}(t) &= \gamma\left(-A(t) + R\left(G(t), Q(t)\right) A\left(t-\tau\right)\right), \\ \dot{G}(t) &= G_0 - \gamma_g G(t) - e^{-Q(t)}\left(e^{G(t)} - 1\right)|A\left(t-\tau\right)|^2, \\ \dot{Q}(t) &= Q_0 - \gamma_q Q(t) - s(1 - e^{-Q(t)})|A\left(t-\tau\right)|^2, \end{aligned} \tag{58}$$

where $R(G,Q) = \sqrt{\kappa}e^{(1-\alpha_g)G/2-(1-\alpha_q)Q/2-i\psi}$, the variable $A(t)$ is complex and denotes the amplitude of the electric field, and the real variables $G(t)$ and $Q(t)$ stand for the saturable gain and loss respectively. For certain parameter values, this system exhibits localized periodic pulses with the period close to τ, see Fig. 20. The emergence of several pulses within the delay interval in this system is studied in [119].

Other examples of solutions that are localized within the delay interval, and hence, localized in the spatio-temporal representation, appeared recently in the papers [120, 121]. In particular, in [120] the authors report solutions which are essentially localized phase defects. The theoretical model which reproduces this effect was shown to be the Ginzburg-Landau equation including an external injection and feedback terms. In the case when the injection and feedback are weak, the model was reduced to the delay equation

$$\frac{d\varphi(t)}{dt} = \Delta - \sin\varphi(t) + \kappa\sin(\varphi(t-\tau) - \varphi(t) - \psi),$$

where Δ, κ, and ψ are parameters. For an appropriate choice of these parameters and a large delay τ, the system exhibits a sharp localized phase jump, which occurs within

every delay interval. By using multiple scale analysis, the authors in [120] derive the amplitude equation in the form of the modified Sine-Gordon equation

$$\frac{\partial A}{\partial \theta} = \sin\bar{\varphi} - \sin\varphi + \frac{\partial A}{\partial x^2} + \tan\psi \left(\frac{\partial A}{\partial x}\right)^2,$$

where $\sin\bar{\varphi} = \Delta - \sin\psi$, x is the pseudo-space and θ is the pseudo-time. As a necessary conditions for the appearance of such a localized solution, the authors mention the combination of the saddle-node bifurcation on a circle and a delayed feedback.

6.8 Spiral defects and turbulence in 2D

Many new challenging problems arise when a system is subject to several delayed feedbacks acting on different timescales [85, 84]. In contrast to the single delay situation, essentially new phenomena occur, related to higher spatial dimensions involved in the dynamics.

A simple paradigmatic setup for the multiple delays case is the following system

$$\dot{z} = az + bz(t-\tau_1) + cz(t-\tau_2) + dz|z|^2, \tag{59}$$

which generalizes the single feedback case (51). Equation (59) describes the interplay of the oscillatory instability (Hopf bifurcation) and two delayed feedbacks, which we consider acting on different timescales $1 \ll \tau_1 \ll \tau_2$. The variable $z(t)$ is complex, and the parameters a, b, and c determine the instantaneous, τ_1-, and τ_2-feedback rates, respectively.

In [85, 84] it is shown that two-dimensional patterns such as spiral defects and defect turbulence are typical of system (59). Moreover, they can be also generically found in a semiconductor laser model with two optical feedbacks.

The main idea is that the spatio-temporal representation (see Sec. 2.1) with 2D spatial domain can be used since the time delays are acting on different timescales. The first spatial coordinate is related to the timescale τ_1, and the second one to τ_2. The corresponding normal form is the 2D Ginzburg-Landau equation (43) with some specific boundary condition (see Sec. 4.4). As a result, the 2D spatiotemporal phenomena known from partial differential equations [91, 79, 80] can be found in delay systems of the form (59).

Figure 21 shows spiral defects and defect turbulence found in Eq. (59). The associated time-series $|z(t)|$ are shown in Figs. 21(d) and 21(e), computed for the parameter values $a = -0.985$, $b = 0.4$, $c = 0.6$, $d = -0.75 + i$, $\tau_1 = 100$, and $\tau_2 = 10000$ for Fig. 21(a,b,d) and the same parameters except $d = -0.1 + i$ for Fig. 21(e,c). These parameter values correspond to the situation where the system is slightly above the instability threshold ($a_{thr} = -1$), and the zero steady state is weakly τ_2-unstable, i.e. the only unstable spectrum is the τ_2-spectrum (see Sec. 3.3).

The time series exhibit oscillations on different timescales related approximately to the delay times. However, the two-dimensional spatio-temporal representation of the data (see Sec. 2.1) in Figs. 21(a-c) reveal the nature of the dynamical behaviors. In

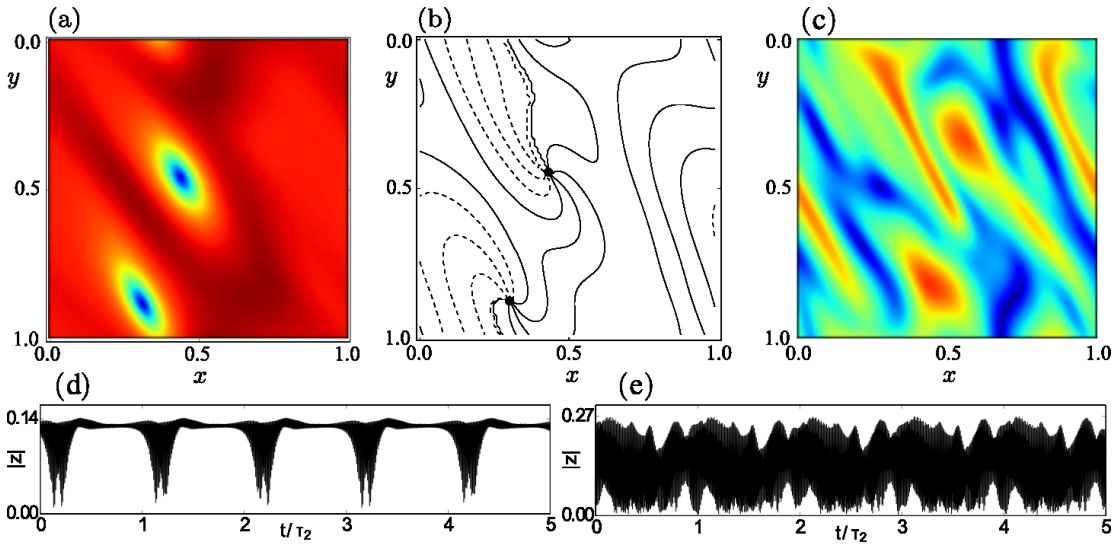

Figure 21: Spiral defects in system with two delays (59). (a-b) 2D spatio-temporal representation of the time series for $|z|$ and the phase of z, respectively, reveals the spiral defects. Shown are snapshots for a fixed value of the pseudo-spatial coordinate θ. In (a), the magnitude of $|z|$ shown in color, and in (b), the constant level lines for the phase are plotted. (c) Similar spatio-temporal representation of the time series for other parameter values (see text for the parameters) of $|z(t)|$ reveals the defect turbulence. (d), (e) Time series corresponding to the defects (a-b) and turbulence (c), respectively.

particular, the first case in 21(a-b) corresponds to a (frozen) spiral defects solution, where the two coexisting spiral defects are shown by the dots. At the defect points, the level lines for the phase meet, the phase is not defined, and $|z| = 0$. The solution shown in Fig. 21(c) corresponds instead to the defect turbulence regime, where the modulation of the amplitude $|z(t)|$ starts to approach the zero level in a random-like manner. The corresponding spatial representation reveals non-regular motions of the spiral defects. The plots are snapshots in time.

Those types of defects and turbulence regimes have been also reported for the Lang-Kobayashi model of a single-mode, semiconductor laser with two optical feedbacks [85].

7 Experiments on long-delay systems

In this section we review a series of experiments on long-delayed feedback systems. Their spatio-temporal nature is disclosed with a proper representation and a rich variety of phenomena appear, which a purely temporal description is unable to show. Most of the experiments described have been performed in optical systems, in particular in laser setups.

7.1 Spatio-temporal chaos and defects turbulence

The effect of a delayed feedback in the case of short delays was investigated in a semiconductor laser (where the propagation delay is naturally relevant because of the short timescales of the system) [37] and in a CO_2 laser [57]. In the former case, a Hopf bifurcation followed by stable oscillations was observed, with frequencies well reproduced by a linear model; in the latter, a far more complicated behavior with period doubling, frequency locking and quasi-periodicity leading to chaos was shown.

Later on, the same group performed a study where the delay time in the feedback loop on the CO_2 laser was greatly increased due to a specific setup [43]. The resulting dynamics showed again a sequence of complicated features, but the analysis of the autocorrelation function indicated the existence of at least two well-separated time scales (see Fig. 22, left). A data reorganization, as pictured in Eq. (3) allowed a clear understanding of the role of the different time scales. The bidimensional pattern obtained (Fig. 22, right), displays a complicated space-like dynamics within a delay cell evolving along the time-like direction.

In that paper, the STR was first introduced and used to describe the spatio-temporal properties on an experimental system with long delay. In such a representation, the features of a transition towards (pseudo) space-time chaos were shown, as a function of a system's parameter.

In a successive work [44], the evidence and characterization of defect-mediated turbulence was shown in the same setup, with a transition to a phase turbulent regime. The time series of the laser intensity evidenced the existence of phase defects, close to a first destabilization of the steady state via a Hopf bifurcation (Fig. 23, left). The STR showed the propagation of the defects structures (Fig. 23, right), with an erratic behavior. For a choice of the parameters, the defects regime was a transient phenomenon,

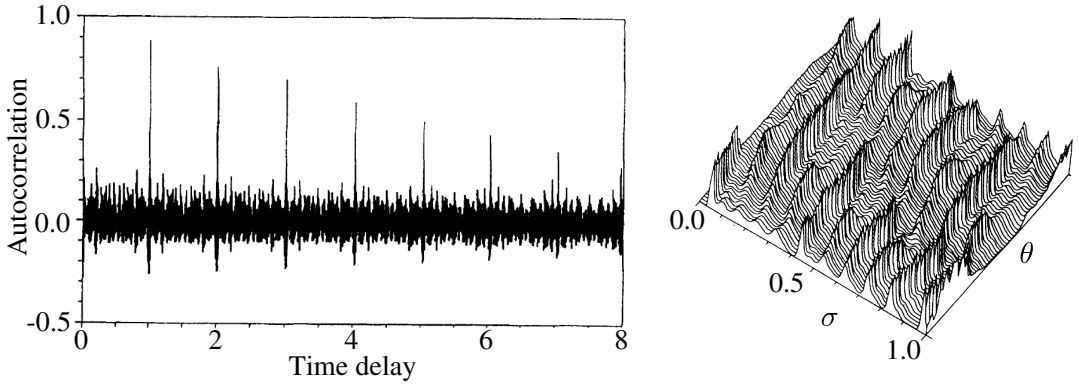

Figure 22: Normalized autocorrelation function of the CO_2 laser intensity (left); the horizontal scale is in units of the delay time. Right: spatio-temporal representation of the signal. (The figure is adapted with permission from Ref. [43]. Copyrighted by the American Physical Society.)

with a scaling of the transient time (in delay units) very close to that predicted for a diffusive behavior in 1D extended systems.

A widely used technique for the control of chaos was introduced by Pyragas [122]. The method employs a delayed variables to stabilize periodic orbits in a chaotic regime. For sufficiently long delays, the investigation of the effect of such a feedback can be studied using the STR. In an experiment with a magneto-elastic beam system under time delayed feedback control [123], such a method has been applied, plotting the displacement as a variable (Fig. 24(a)) and the corresponding STR (Fig. 24(b)).

The autocorrelation function and its structure has been proven to be a powerful tool to characterize the long-delayed systems; conversely, the existence of well defined features such that the presence of revivals and the indication of a drifting is a signature of the possible spatio-temporal dynamics.

An example of the use of this indicator is presented in a study of an experiment carried out in a Vertical Cavity Surface Emitting Laser (VCSEL) with polarized optical feedback [55]. The autocorrelation function of the laser intensity signal displays the revivals at almost the multiples of the delay time τ_c (Fig. 25 (left) and the inset). In this work, it is suggested to use the STR for the autocorrelation function (Fig. 25, right): the averaging process of the autocorrelation allows to display features (in this case, a drift) which are otherwise hidden by the small timescales and the low signal-to-noise ratio. The delay time was $\tau_c = 3.63\ ns$, much longer of the scales of spiking dynamics typical for the optical feedback system which is in the *ps* range.

A further step has been taken in understanding the properties and using the features of the autocorrelation function in Ref. [54]. There, the study of a simple linear, stochastic model allowed both to reproduce the experimental findings from a semiconductor laser with an optical feedback (see Fig. 26) and to evaluate the drift in terms of phenomenological parameters.

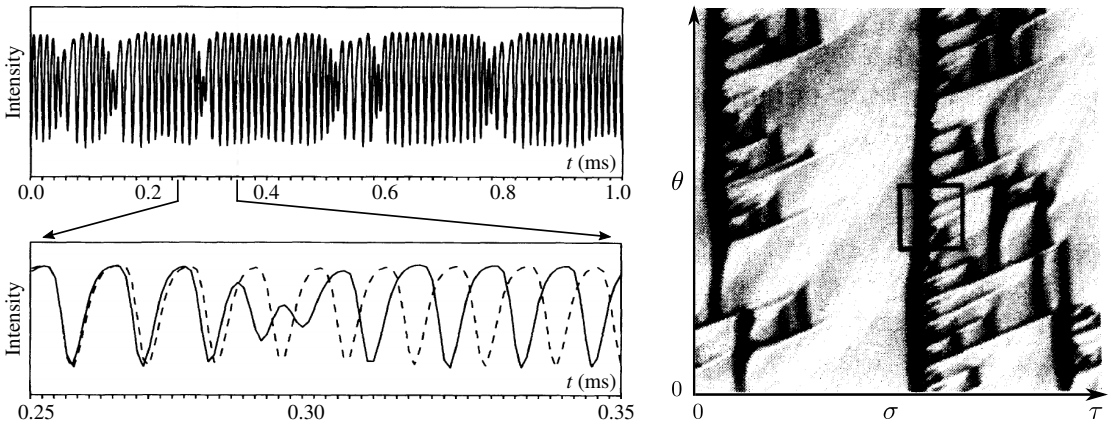

Figure 23: Temporal series of the CO_2 laser intensity, showing the existence of phase defects (left). Right: spatio-temporal representation of the signal; the horizontal scale is one delay time, the vertical is the pseudo time. (The figure is adapted with permission from Ref. [44]. Copyrighted by the American Physical Society.)

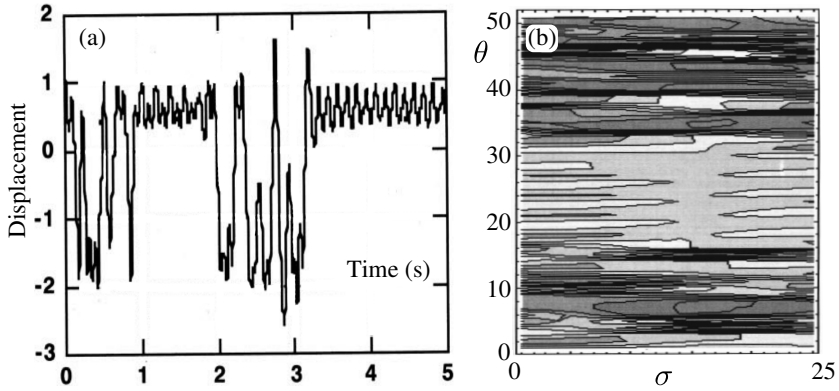

Figure 24: (from [123]) Dynamics of magneto-elastic system with delayed feedback control; (a) displacement, (b) contour plot of waves on the spatiotemporal state space. (Reprinted from [T. Hikihara and Y. Ueda, "An expansion of system with time delayed feedback control into spatio-temporal state space", Chaos 9, 4 (1999), pp. 887-892], with the permission of AIP Publishing.)

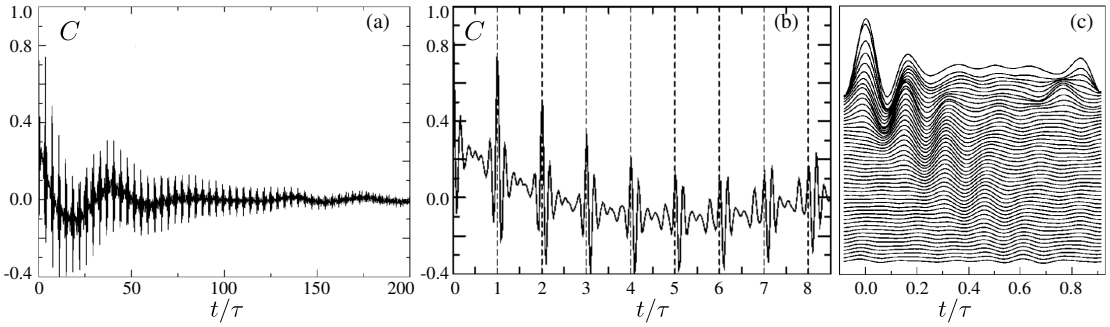

Figure 25: Autocorrelation function of VCSEL intensity (a), its zoom (b), and spatio-temporal representation (c). (The figure is adapted with permission from Ref. [55]. Copyrighted by the American Physical Society.)

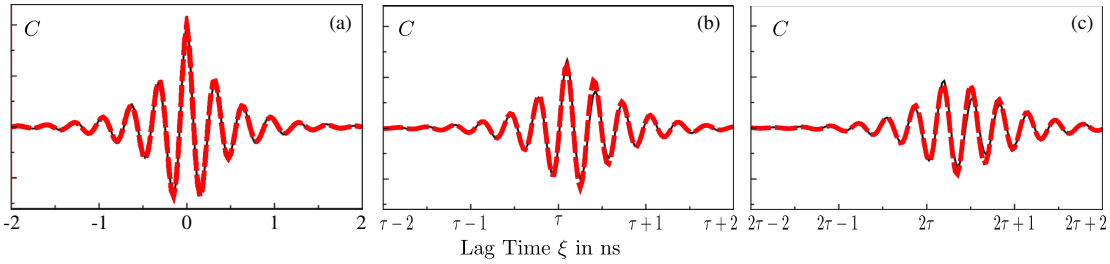

Figure 26: (color online) The central peak (a) and the first two delay echoes [(b) and (c), respectively] of the autocorrelation of a semiconductor laser subject to delayed feedback. The solid thin line shows the experimental data and the dashed lines correspond to the fitted analytic expressions from a linear stochastic model. (The figure is adapted with permission from Ref. [54]. Copyrighted by the American Physical Society.)

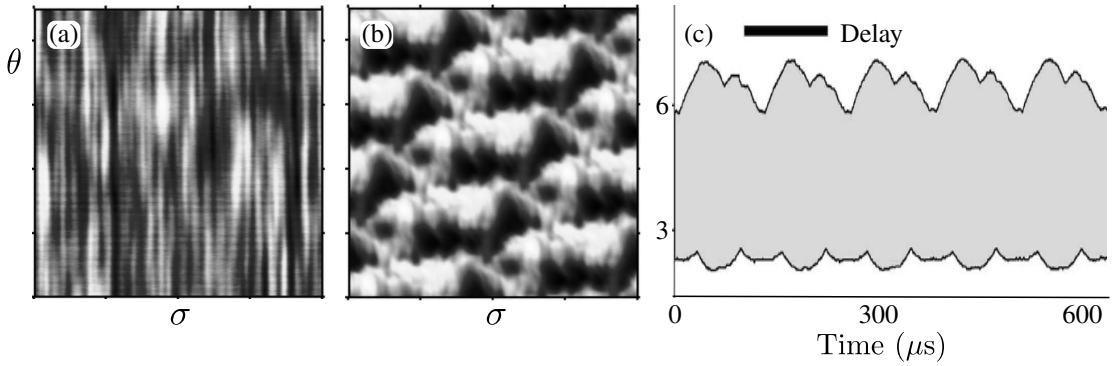

Figure 27: Spatio-temporal representations of the intensity dynamics for a laser with (a) no feedback and (b) with the delayed feedback. (c) Envelope of the time series of the intensity dynamics: the bar shows the delay τ. (The figure is adapted with permission from Ref. [124]. Copyrighted by the American Physical Society.)

A fiber ring laser, with a feedback loop realized with an additional fiber ring cavity may represent a convenient, all-optical dynamical system for studying the effect of long delays. In Ref. [124] this setup produced a large variety of behaviors ranging from the typical phenomenology expected in short delays, with frequency locking and low dimensional chaos, to pattern formation and structure propagation typical for spatio-temporal systems (Fig. 27(b)). An extension to the case of two long-delayed coupled lasers is also studied. In Fig. 27(c), example of time series is shown indicating how the multiple time scales of the system are folded in the dynamics. In such a system, a suitable decomposition in terms of the Karhunen-Loevè modes allowed to estimate some of the statistical indicators of complexity (such as the entropy) and their scaling with the delay time.

7.2 Front dynamics: coarsening, nucleation, and pinning

A hysteresis and a diffusive coupling are the main ingredient for the so-called bistable reaction-diffusion systems (see e.g. [125]). A bistable VCSEL with a long-delayed opto-electronic feedback has shown to present most of the features of the reaction-diffusion systems [100]. Depending on the parameters, the formation and annihilation of pairs of fronts was observed, with coarsening towards a homogeneous (strong) state (see Fig. 28). The characterization of the drift in terms of the fronts motions and its estimation using a simple model has been also provided, as a further evidence of the typical behavior of long delayed systems.

The phenomenon of nucleation has been also observed [100, 101]: the formation of localized buds of the strong phase into regions of the weak one (Fig. 28, right panel).

A mechanism for stabilizing temporal domain walls away from the Maxwell point, based on antiperiodic regimes in a delayed system close to a bistable situation, leads to a cancellation of the average drift velocity. As a consequence, the coarsening mechanism is blocked. The results are demonstrated [53] in a normal form model and experimentally

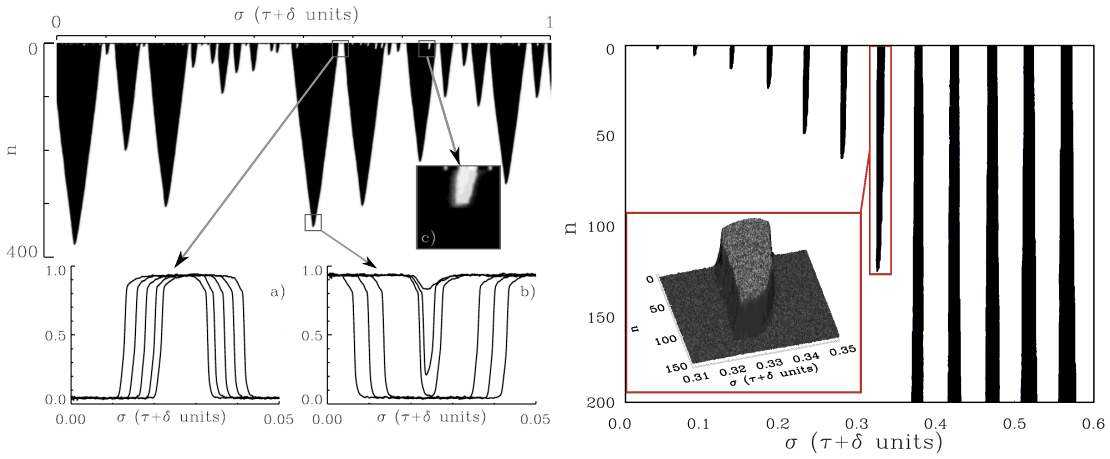

Figure 28: Left: Spatio-temporal representation of the polarized laser intensity showing coarsening towards the lower state (white), with fronts creation (a) and annihilation (b), as well as nucleation of the strong state into the weak one (c). Right: Spatio-temporal representation illustrating nucleation for different initial pulse widths. (The figure is adapted with permission from Ref. [101]. Copyrighted by the American Physical Society.)

in a laser with optical injection and delayed feedback. In Fig. 29, it is shown how a STR using a pseudo space cell of different lengths (here $2\tau$is used) allows to recover the standard information about the propagation of the patterns. In this case, the coarsening is blocked and the structures propagate without shrinking or expanding, as seen also in Fig. 29(c) in the case of the creation of new domains. For different parameter values, a standard coarsening regime is shown.

The application of a modulated signal produced another typical phenomenon of extended systems: the pinning/unpinning of localized structures [126]. The phenomenon has been shown experimentally in the setup of [100], with the addition of a periodic modulation on the pump of the VCSEL; a study on a phenomenological model also confirmed the features of the measurements. In Fig. 30, the experiment evidences the unpinning changing the asymmetry parameter of the bistable states. For small values, the fronts do not propagate at all and the growth rate is zero. Above a first threshold, the growth rate suddenly increases with a square-root scaling, indicating that the unpinning transition has occurred. However, only the left front is propagating, whereas the right front is still pinned [see inset (a)]. The situation remains qualitatively unaltered until a second bifurcation takes place, illustrated by the abrupt change in the growth rate. This corresponds to the unpinning of the right front [inset (b)]. The other front now also drifts away, such that the high power state invades the whole system.

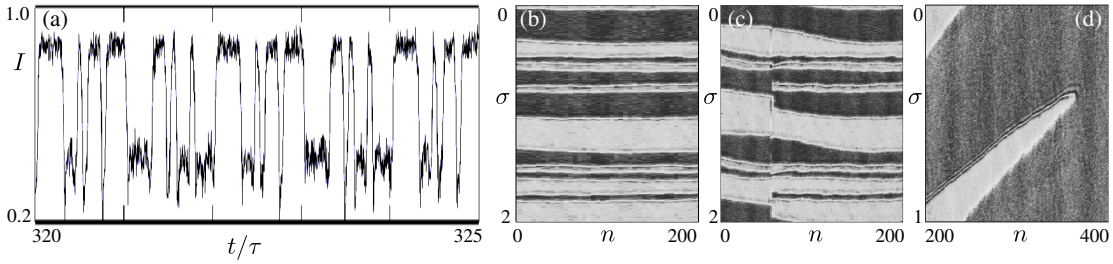

Figure 29: (a) Time series of the laser intensity and spatio-temporal representation using a spatial cell of length 2τ (b,c). Example of domain creation and propagation without coarsening (c); for other parameters, coarsening occurs (d). (The figure is adapted with permission from Ref. [53]. Copyrighted by the American Physical Society.)

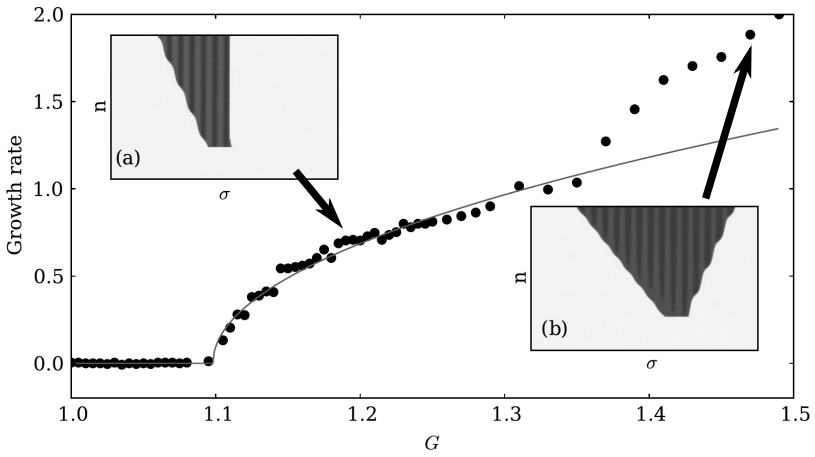

Figure 30: Pinning regimes, illustrated in terms of the growth rate of the dominant phase against the bistable states asymmetry parameter G. Solid line: square-root fit in the range $1 \leq G \leq 1.3$. Insets: Space-time representation of the laser intensity for $G = 1.2$ [(a)] and $G = 1.47$ [(b)]. (The figure is adapted with permission from Ref. [126]. Copyrighted by the American Physical Society.)

7.3 Strong and weak chaos

The experimental demonstration of the existence of an anomalous (strongly unstable, see Sec. 3) Lyapunov exponent represents a difficult task. The scaling of the maximal exponent with the delay time cannot be simply revealed by a visual inspection of the patterns or even from the evidence of small amplitudes of the autocorrelation revivals. In fact, the evidence of a transition between a dynamics with almost coherent propagation in the pseudo time to a locally strong, chaotic represents only an indication of the possible existence of the anomalous exponent.

The notion of strong and weak chaos was introduced in [65], discussing the dynamics of complex networks with delayed couplings. The authors distinguished the two regimes by the scaling properties of the maximum Lyapunov exponent: the existence of an anomalous exponent corresponds to the strong chaos regime (see Sec. 6.4 for more details). It was shown that this is related to the condition for stable or unstable chaotic synchronization. The concept is illustrated in simulations of laser models and in experiments with coupled electronic circuits, and the transitions from weak to strong chaos and vice versa changing the coupling strength are described. The analysis of the stability of synchronization between two units shows that chaos is weak if and only if the two units can be synchronized. Hence, it represents a less demanding condition for checking the existence of the anomalous LE. Figure 31(a) shows the simulated LEs in comparison with the experimentally measured cross-correlation C between the maxima of the time series of the two electronic circuits as a function of the coupling strength. For small coupling, zero-lag synchronization of periodic dynamics is observed. If the coupling is increased, the dynamics becomes chaotic while complete synchronization is maintained. With a further increase of the parameter, the cross correlation first decreases and then increases again until synchronization is reached once more, indicating transitions from weak to strong chaos and back to weak chaos.

In [69] a detailed study of an experiment with a semiconductor laser with optical feedback and a corresponding model (Lang-Kobayashi equations [14]) showed a good indication that the system could present a transition between weak and strong chaos (see e.g. Fig. 31(b-c)). While the reported results are not definitive, the possibility of a characterization of the strong chaos regime in a fast, optical system is promising, even in view of possible statistical analysis given the huge numbers of samples that can be collected in a single measurement.

In the same setup, a different approach is presented in [70]. The study focuses on a characterization based on the consistency indicator: it estimates the reproducibility of responses of a dynamical system when repeatedly driven by similar inputs, starting from different initial conditions. The feedback loop is realized with an optical fiber that can be switched between two very different length configurations. At first, the laser if feed back via the shorter loop, while the second acts as an optical memory storing the output of the laser (configuration A). Then, the shorter loop is excluded and the longer starts to feed the laser, injecting the field stored before (configuration B). The results show that the laser can exhibit different and independent responses to the same drive depending on the dynamical regime, indicating different levels of consistency; this

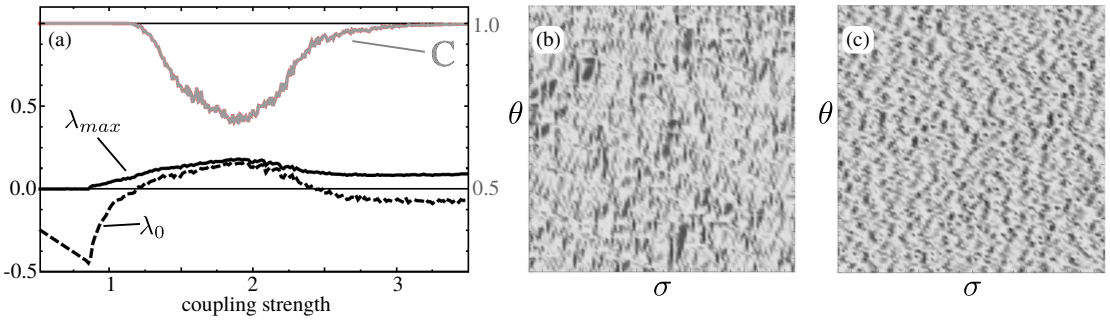

Figure 31: (a) Simulated and maximal $\lambda_{\max}$ (solid line) and instantaneous λ_0 (dashed line) Lyapunov exponents of two electronic circuits and experimentally measured cross-correlation C [gray line] between the maxima of the time series versus coupling strength. (b-c): Space-time diagram of a laser intensity for a single laser with a self-feedback of $\tau = 10ns$. Panel (b) corresponds to weak chaos and (c) to strong chaos. (The figure is adapted with permission from Refs. [65] and [69]. Copyrighted by the American Physical Society.)

can be see also by comparing the spatiotemporal patterns in the configurations A-B. A transverse Lyapunov analysis, carried out on the experimental data and compared with simulations, leads to the conclusion that the consistent regimes can be related to the presence of the weak chaos, and the inconsistent ones corresponding to a strong chaos regime.

An experimental characterization of the mechanism for the emergence of strong chaos was studied in [127]. The authors also demonstrate certain similarity properties of the dynamics, relating different pump currents regimes, to the feedback strength that can be adjusted in such a way that the dynamics is similar.

7.4 Reservoir computing

Recently, time delayed systems with long time delays are used successfully for reservoir computing [128]. The space-time representation for the processing response of the reservoir has been presented in [129, 130], showing that it is indeed suited to the matrix operation which is typically involved at the readout layer of reservoir computing processing. The representation also well illustrates how a delay-based reservoir computer emulates a network of virtual neurons, with which the reservoir computing concept can be implemented in delay systems. In Fig.32, a space-time plot is presented for the processing of a spoken digit ("eight"), in a speech recognition task.

7.5 Chimera states

The increasing interest in the investigation of complex systems, either spatially extended or on a network, has lead recently to the introduction of previously unexpected states, named *chimeras*. Such states are characterized by the coexistence, in a large set of

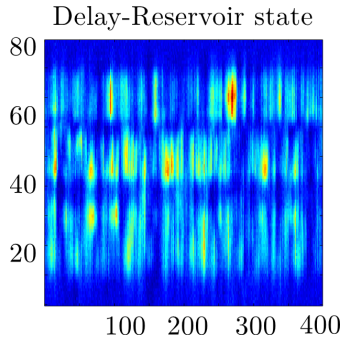

Figure 32: Space-time representation of reservoir computing network input; the color encodes the amplitudes of the signals, with red (blue) corresponding to large (small) values. The horizontal axis is the delay time, the vertical the number of delays. (The figure is kindly provided by L. Larger, similar to that in [129])

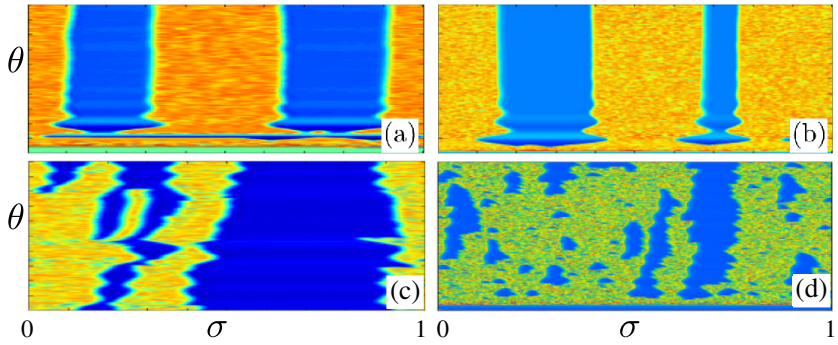

Figure 33: (from [132] and [134], color online) Two-headed chimera, (a) experiment and (b) numerics. Turbulent motion, (c) experiment and (d) numerics. (Reprinted (figure) with permission from [L. Larger, B. Penkovsky, Yu. Maistrenko, Phys. Rev. Lett. 111, 054103, 2013.] Copyright (2013) by the American Physical Society.)

identical oscillators, of two separated groups evolving synchronously and incoherently respectively despite a homogeneous coupling [131].

In [132, 133], time delayed systems are found to display temporal patterns which split into regular and chaotic components repeating within a delay unit; in the corresponding pseudo space-time representation, the behavior is found to show the features of a chimera state (see Fig. 33). This phenomenon results from a strongly asymmetric nonlinear delayed feedback driving a highly damped harmonic oscillator dynamics. The physical experiment corresponds to a bandpass frequency modulation (FM) delay oscillator. Numerous virtual chimera states are obtained and analyzed, through experiment, theory, and simulations.

The report on a highly controllable experiment on chimeras, based on an optoelectronic delayed feedback applied to a wavelength tunable semiconductor laser, is presented in [134]. There, a wide variety of chimera patterns are investigated and interpreted. A

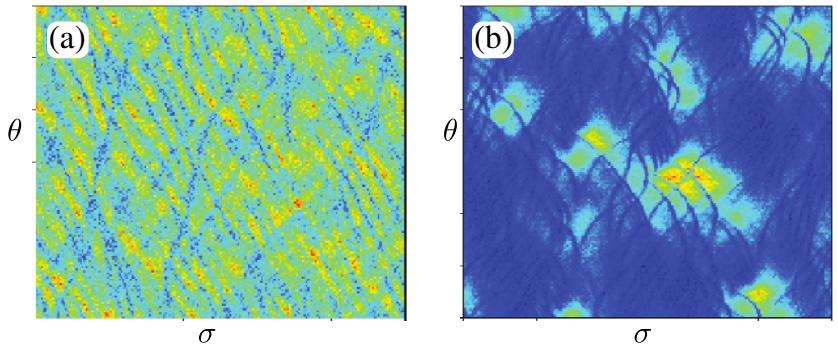

Figure 34: (from [135], color online) Coherent structures in spatiotemporal dynamics in experiment for laminar and turbulent regimes of fiber laser. Space-time diagram of intensity for the laminar (a) and turbulent regime (b). Adapted by permission from Macmillan Publishers Ltd: Nature Photonics (G. Turitsyna et al. "The laminar-turbulent transition in a fibre laser", Nat. Photon. 7, 10, pp. 783–786.), copyright (2013).

cascade of higher-order chimeras as a pattern transition from increasing number of clusters of chaoticity is uncovered. Moreover, as the gain increases, the chimera state is gradually destroyed on the way to apparent turbulence-like system behavior.

7.6 Optical cavity dynamics of localized excitations

The study of optical cavity dynamics can be approached in two different ways. The first is to use the Maxwell-Bloch equations with a suitable modeling of the nonlinear processes involved in the gain medium and imposing appropriate boundary conditions which amounts to provide a set of non-local conditions (delay difference map) for the field. The second way is to introduce a phenomenological model based on delay equations which can represent an approximate description of the dynamics, as multiple reflections at retarded times occur. A typical example of the latter is the Lang-Kobayashi model, which takes into account only the first of the multiple (in principle, infinite) reflections from the distant mirror assuming a small feedback gain.

Examples of complex dynamics in laser cavities are reported in the literature. However, only recently the progresses in high temporal resolution acquisition allowed to follow the microscopic evolution of the field, possibly representing it in a spatio-temporal representation and indicating the possibility of a description in terms of delay models.

A fiber laser operating in laminar and turbulent regimes is investigated in [135]. The transition from a linearly stable coherent laminar state to a highly disordered state of turbulence is shown as spatial size or the strength of excitation increases. In the paper, it is evidenced that the laminar phase is analogous to a one-dimensional coherent condensate using a spatio-temporal representation (see Fig. 34) and that the onset of turbulence is due to the loss of spatial coherence.

A report about a weak interaction of solitons is presented in [136]. The experiment studies temporal optical cavity solitons injected and recirculating in a coherently driven

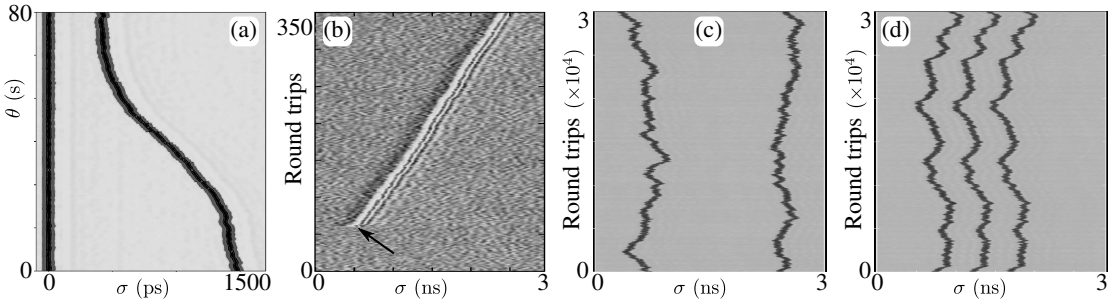

Figure 35: (from [136, 120, 121]) (a): Long-range interactions of a pair of cavity solitons. The temporal evolution of two cavity solitons is shown in a spatio-temporal representation: the horizontal axis is the cavity time variable, the vertical is the number of cavity roundtrips. The initial separation is 1500 ps (577 soliton widths), the interaction is attractive until a stable separation of 420 ps is attained [136]. (b): Nucleation of phase bits in space-time representation [120]. A phase perturbation is applied (shown by arrow) while the system is in a stable stationary locked state. Following that perturbation, a pulse is nucleated and repeats with a periodicity close to the feedback delay time. (c) and (d): Space–time representation of the motion of dissipative solitons (DS) in different situations [121]. (c): Two independent DS. (d): A 3-DS molecule. Adapted by permission from Macmillan Publishers Ltd: Nature Photonics (J. K. Jang et. al., "Ultraweak long-range interactions of solitons observed over astronomical distances", Nat. Photon. 7, 8, pp. 657–663.), copyright (2013); Nature Communications (B. Garbin et al., "Topological solitons as addressable phase bits in a driven laser", Nat. Commun. 6, pp. 5915), copyright (2015); Nature Photonics (M. Marconi et al., "Vectorial dissipative solitons in vertical-cavity surface-emitting lasers with delays", Nat. Photon. 9, pp. 450–455), copyright (2015).

passive optical-fiber ring resonator. Pairs of solitons are observed interacting over a range as large as 8,000 times their width. In the most extreme case, their temporal separation changes as slowly as a fraction of an attosecond per roundtrip of the 100-m-long resonator, or equivalently 1/10,000 of the wavelength of the soliton carrier wave per characteristic dispersive length. The interactions are so weak that, at the speed of light, an effective propagation distance of the order of an astronomical unit can be required to reveal the full dynamical evolution (see Fig. 35(a)). A model is discussed also, employing a modified Lugiato-Lefever equation [137] using the slow (number of roundtrips) and fast (roundtrip variable) times as equivalent time and space variables respectively.

It is shown both theoretically and experimentally in [138] how lasing localized solitons form out of a passive mode-locked semiconductor laser. The way the pulses become localized, and can be used for storing information as independent addressable bits within a cavity trip time is presented and discussed.

In [120] an experimental and analytical demonstration is reported of the existence of longitudinal localized states in the phase of laser light. They represent robust and

versatile phase bits that can be individually nucleated (see Fig. 35(b)) and canceled in an injection-locked semiconductor laser, operated in a neuron-like excitable regime and subjected to delayed feedback. The observations are analyzed in terms of a generic model, which confirms the topological nature of the phase bits and discloses their analogy with Sine–Gordon solitons.

The nonlinear polarization dynamics of a vertical-cavity surface-emitting laser placed in an external cavity lead to the emission of temporal dissipative solitons [121]. The vectorial character is a consequence of the fact that they appear as localized pulses in the polarized output, but leave the total intensity constant. When the cavity roundtrip time is much longer than the soliton duration, several independent solitons as well as bound states (molecules) may be hosted in the cavity (see Fig. 35). All these solitons coexist together and with the background solution. The experimental results are well described by a theoretical model that can be reduced to a single delayed equation for the polarization orientation, which allows the vectorial solitons to be interpreted as polarization kinks. A Floquet analysis is used to confirm the mutual independence of the observed solitons.

Recently, a photonic regenerative memory based upon a neuromorphic oscillator with a delayed self-feedback has been shown and discussed in [139]. The existence of a temporal response characteristic of localized structures enables them as bits in an optical buffer memory aimed to storage and reshaping of data information. The experimental implementation, based upon a nanoscale nonlinear resonant tunneling diode driving a laser, is supported by the analysis of the paradigm of neuronal activity, the FitzHugh-Nagumo model with delayed feedback.

8 Conclusions and perspectives

The dynamics of systems with feedback is invariably modified by the presence of a further timescale, related to the signal propagation in the feedback loop. In many situations, the evolution is on very slow scales and such effect is negligible; however, this is not always the case. From optical setups, to neuroscience and complex networks a relevant delay in the re-entering informations often causes sensible effects such as multistability, quasi-periodicity, and several routes to chaos.

Particularly for long delays the observed behaviors appear high-dimensional. In that case, roughly defined as the situation when the delay time is much longer than other internal timescales, completely new phenomena can be observed where purely temporal phenomena manifest complex behaviors at different timescales.

The first studies recognized the value of the auto-correlation function for the preliminary analysis of the time series. Multiple recurrence peaks evidenced the relevant timescales involved: accordingly, a re-organization of the data provided a successful comparison of the dynamics with that of an equivalent spatially extended system. The spatio-temporal representation obtained in such a way is a fast and useful tool for identifying the features hidden in the data. The method has proven to be very successful and many applications of it have been presented, disclosing the interpretation of quite com-

plicated temporal patterns in terms of well established spatio-temporal phenomena. As examples, defects, space-time intermittency, fronts, coarsening and nucleation, pinning and unpinning, chimeras, solitons creation, propagation, clustering and annihilation, spirals, etc. have been demonstrated both in models and experiments on long delay systems. The spatio-temporal representation also illustrates the systematic presence of a drift in the information propagation. This element, signature of the causality principle, has been suitably formalized using the maximum comoving Lyapunov exponent.

The proper characterization of long delay system has been the subject of a copious amount of papers. Beyond phenomenological evidences, strong efforts to define their properties have been pursued in terms of statistical and dynamical indicators. Starting with simple discrete models, the main features of the Lyapunov spectrum have been studied in details showing the peculiarity of the long delay systems. In particular, the Lyapunov spectrum and its scaling with the delay time has permitted to establish the latter quantity as the system size, leading to a clear analogy with spatially extended systems. A classification of the instabilities found in long delay systems and their connection to the equivalent ones in spatially extended systems has been discussed. Besides, the scaling of the main nonlinear indicators such as Kolmogorov-Sinai entropy and the Kaplan-Yorke dimension have also been computed.

In the study of Lyapunov spectrum, already in the earlier works and in the recent years a very important topic appeared. The elements of the discrete subset of the Lyapunov spectrum may behave differently (the anomalous, strongly unstable spectrum) with respect to the rest, featuring what is probably one of the most distinctive character of the long delay systems: the strong and weak chaos regimes. This classification scheme is at the very basics of the correspondence with a spatio-temporal dynamics. Given the importance of the distinction between the strong and weak chaos, some key questions remain open. Among them, can those regimes be determined by different, and more direct criteria than a Lyapunov analysis? We remark also, that in the event of the presence of anomalous exponents the long delay systems can be considered as the bridge between low dimensional and high-dimensional, spatio-temporal-like systems. Further investigations in the features of such passage are of importance for the subject.

Another point to stress is the connection between the weak/strong chaos and an associated synchronization transition in delay coupled networks. Indeed, in the strong chaos regime the linearized model is formally the same of that considered in the framework of chaos synchronization to determine the sub-Lyapunov exponents. The possible change of sign of these anomalous exponents could be therefore interpreted as the signature of synchronization with the delay forcing, thus permitting a meaningful description in terms of a smooth pseudo spatio-temporal evolution.

The long delay systems are intrinsically multiscale: the existence of the long feedback timescale is at the basis of the very features of the dynamics, and represents the key factor for the whole picture. A rigorous approach to the equivalence with spatially extended systems is properly pursued with the aid of multiple timescales techniques. The exact derivation of the Ginzburg-Landau normal form has been provided in such a way, studyng several models with long delay in the vicinity of a a destabilization. However, only in a limited number of cases a rigorous proof has been given. A challenging task is

to extend it to other situations, with possible mappings to normal forms other than the Ginzburg-Landau.

Recognizing the fundamental role of the multiple timescales in long delays system leads naturally to a generalization of the approach when more than a single feedback loop, and therefore one delay term, is part of the system. It has been shown that the situation of diverse, hierarchically-long delays can be treated in a very similar way. However, the mapping with spatio-temporal systems becomes more complicated and the space-like variables involved are related to the number of delay times considered, each acting on well-separated scales. Even in the simple case of two delays, very complicated temporal patternings may occur; the suitable representation, now keeping into account a vectorial drift, shows the occurrence of peculiar bidimensional phenomena such as spirals and topological defects. How a general approach can be pursued in different situations, and which are the possible phenomena expected therein, is a topic of great interest given the growing effort to describe system with complex connected interactions, e.g. biological, social and financial networks. As a consequence, we would expect the occurrence of the temporal analogue of even more complicated spatio-temporal phenomena such as line-defects in 3D systems and their motions.

Delayed effects are widespread in many complex situations, and the way the signal propagates could also be related to the instantaneous configuration of the setup which can change with time. The field of state-dependent delay systems represents a further, challenging topic which could benefit as well of the present approach.

When real systems are investigated, the influence of noise is unavoidable, and it is very important to study its effects on delay systems with long delays. Many questions are still open, for example, how the generically increasing multistability of delay systems can interplay with noise and whether the observed peculiar scaling behaviors could be analogous to those of noisy spatio-temporal systems.

A growing number of studies are appearing on long delay systems, many of them are experimental investigations. The possibility to unveil an elegant mechanism at the very basis of quite complicated temporal sequences is a powerful tool and can greatly motivate the research. We expect even more groups treating non-local interactions in a proper way and considering the idea of a space-time equivalence. Many fields could benefit from embracing this approach, paving the way for a systematic classification of setups and physical phenomena into well-established spatio-temporal, dynamical categories.

Acknowledgments We acknowledge fruitful collaborations and discussions with many collegues; among them, F. T. Arecchi, S. Barland, I. Fischer, M. Giudici, L. Larger, S. Lepri, F. Marino, A. Mielke, A. Politi, G.P. Puccioni, K. Schneider, M. Wolfrum, M. Zaks. We thank the German Research Foundation (DFG) for financial support in the framework of the Collaborative Research Center 910.

References

[1] M. C. Mackey, L. Glass, Oscillation and chaos in physiological control systems, Science 197 (1977) 287.

[2] O. V. Popovych, C. Hauptmann, P. A. Tass, Control of neuronal synchrony by nonlinear delayed feedback., Biol Cybern 95 (1) (2006) 69–85. doi:10.1007/s00422-006-0066-8.
URL http://dx.doi.org/10.1007/s00422-006-0066-8

[3] E. M. Izhikevich, Polychronization: Computation with spikes, Neural Computation 18 (2006) 245–282.

[4] K. Ikeda, Multiple-valued stationary state and its instability of the transmitted light by a ring cavity system, Opt. Commun. 30 (1979) 257.

[5] T. Erneux, Applied Delay Differential Equations, Vol. 3 of Surveys and Tutorials in the Applied Mathematical Sciences, Springer, 2009.

[6] M. C. Soriano, J. García-Ojalvo, C. R. Mirasso, I. Fischer, Complex photonics: Dynamics and applications of delay-coupled semiconductors lasers, Rev. Mod. Phys. 85 (2013) 421–470. doi:10.1103/RevModPhys.85.421.
URL http://link.aps.org/doi/10.1103/RevModPhys.85.421

[7] M. Sciamanna, K. A. Shore, Physics and applications of laser diode chaos, Nat. Photon. 9 (3) (2015) 151–162.
URL http://dx.doi.org/10.1038/nphoton.2014.326

[8] Y. Kuang, Delay Differential Equations with Applications in Population Dynamics, Vol. 191 of Mathematics in science and engineering, Academic Press, 1993.

[9] W. Kopylov, C. Emary, E. Schöll, T. Brandes, Time-delayed feedback control of the Dicke–Hepp–Lieb superradiant quantum phase transition, New Journal of Physics 17 (1) (2015) 013040.
URL http://stacks.iop.org/1367-2630/17/i=1/a=013040

[10] G. Orosz, R. E. Wilson, G. Stepan, Traffic jams: dynamics and control, Phil. Trans. R. Soc. A 368 (2010) 4455–4479. doi:doi:10.1098/rsta.2010.0205.

[11] L. Page, Is a moving mass retarded by the reaction of its own radiation?, Phys. Rev. 11 (1918) 376–400. doi:10.1103/PhysRev.11.376.
URL http://link.aps.org/doi/10.1103/PhysRev.11.376

[12] J. D. Jackson, Classical Electrodynamics, Wiley, New York, 1975.

[13] J. De Luca, Electrodynamics of helium with retardation and self-interaction effects, Phys. Rev. Lett. 80 (1998) 680–683. doi:10.1103/PhysRevLett.80.680.
URL http://link.aps.org/doi/10.1103/PhysRevLett.80.680

[14] R. Lang, K. Kobayashi, External optical feedback effects on semiconductor injection laser properties, IEEE J. Quantum Electron. 16 (1980) 347–355.

[15] J. D. Farmer, Chaotic attractors of an infinite-dimensional dynamical system, Physica D 4 (1982) 366–393.

[16] A. D. Myshkis, General theory of differential equations with retarded arguments, Uspekhi Mat. Nauk 4 (5(33)) (1949) 99–141.

[17] R. Bellman, K. Cooke, Differential difference equations, Academic Press, New-York – London, 1963.

[18] S. P. Kuznetsov, Complex dynamics of oscillators with delayed feedback (review), Radiophysics and Quantum Electronics 25 (1982) 996–1009.

[19] J. K. Hale, S. M. V. Lunel, Introduction to Functional Differential Equations, Springer-Verlag, 1993.

[20] O. Diekmann, S. A. van Gils, S. M. V. Lunel, H. O. Walther, Delay Equations: Functional-, Complex-, and Nonlinear Analysis, Springer, 1995.

[21] Various, Complex Time-Delay Systems Theory and Applications, Springer, 2010.

[22] S. Guo, J. Wu, Bifurcation Theory of Functional Differential Equations, Vol. 184 of Applied Mathematical Sciences, Springer-Verlag New York, 2013.

[23] J. Mallet-Paret, Negatively invariant sets of compact maps and an extension of a theorem of cartwright, Journal Of Differential Equations 22 (1976) 33 l–348.

[24] J. Mallet-Paret, R. D. Nussbaum, Global continuation and asymptotic behaviour for periodic solutions of a differential-delay equation, Annali di Matematica Pura ed Applicata 145 (1986) 33–128.

[25] E. V. Grigorieva, S. A. Kashchenko, N. A. Loiko, A. M. Samson, Nonlinear dynamics in a laser with a negative delayed feedback, Physica D 59 (1992) 297.

[26] E. V. Grigorieva, S. A. Kashchenko, Complex temporal structures in models of a laser with optoelectronic delayed feedback, Opt. Commun. 102 (1993) 183.

[27] E. V. Grigorieva, S. Kashchenko, Regular and chaotic pulsations in laser diode with delayed feedback, Int. J. of Bifurcation & Chaos 3 (1993) 1515.

[28] S. A. Kashchenko, The Ginzburg-Landau equation as a normal form for a second-order difference-differential equation with a large delay, Computational Mathematics and Mathematical Physics 38 (1998) 443–451.

[29] I. Kashchenko, S. Kaschenko, Normal and quasinormal forms for systems of difference and differential-difference equations, Communications in Nonlinear Science and Numerical Simulation 38 (2016) 243–256.

[30] T. Vogel, Theorie des Systemes Evolutifs, Gauthier-Villars, Paris (France), 1965.

[31] C. Chicone, Inertial and slow manifolds for delay equations with small delay, J. Differential Equations 190 (2003) 364–406.

[32] L. Kotomtseva, N. Loiko, A. Samson, Development of irregular auto-oscillations in a nonlinear system with lagging, Phys. Lett. A 110 (1985) 339.

[33] M. L. Berre, E. Ressayre, A. Tallet, H. M. Gibbs, High-dimension chaotic attractors of a nonlinear ring cavity, Phys. Rev. Lett. 56 (1986) 274.

[34] K. Ikeda, K. Matsumoto, High-dimensional chaotic behavior in systems with time-delayed feedback, Physica D 29 (1-2) (1987) 223–235. doi:http://dx.doi.org/10.1016/0167-2789(87)90058-3.

[35] B. Dorizzi, B. Grammaticos, M. L. Berre, Y. Pomeau, E. Ressayre, A. Tallet, Statistics and dimension of chaos in differential delay systems, Phys. Rev. A 35 (1987) 328.

[36] M. Le Berre, E. Ressayre, A. Tallet, H. M. Gibbs, D. L. Kaplan, M. H. Rose, Conjecture on the dimensions of chaotic attractors of delayed-feedback dynamical systems, Phys. Rev. A 35 (9) (1987) 4020–4022. doi:10.1103/PhysRevA.35.4020.

[37] G. Giacomelli, M. Calzavara, F. Arecchi, Instabilities in a semiconductor laser with delayed optoelectronic feedback, Opt. Commun. 74 (1989) 97.

[38] S. Lepri, G. Giacomelli, A. Politi, F. T. Arecchi, High-dimensional chaos in delayed dynamical systems, Physica D 70 (1993) 235–249. doi:10.1016/0167-2789(94)90016-7.

[39] G. Giacomelli, S. Lepri, A. Politi, Statistical properties of bidimensional patterns generated from delayed and extended maps, Phys. Rev. E 51 (1995) 3939. doi:10.1016/0167-2789(94)90016-7.

[40] M. W. Lee, L. Larger, V. Udaltsov, Éric Genin, J.-P. Goedgebuer, Demonstration of a chaos generator with two time delays, Opt. Lett. 29 (4) (2004) 325–327. doi:10.1364/OL.29.000325.
URL `http://ol.osa.org/abstract.cfm?URI=ol-29-4-325`

[41] Y. Chembo Kouomou, P. Colet, L. Larger, N. Gastaud, Chaotic breathers in delayed electro-optical systems, Phys. Rev. Lett. 95 (2005) 203903. doi:10.1103/PhysRevLett.95.203903.
URL `http://link.aps.org/doi/10.1103/PhysRevLett.95.203903`

[42] R. Lavrov, M. Peil, M. Jacquot, L. Larger, V. Udaltsov, J. Dudley, Electro-optic delay oscillator with nonlocal nonlinearity: Optical phase dynamics, chaos, and synchronization, Phys. Rev. E 80 (2009) 026207. doi:10.1103/PhysRevE.80.026207.
URL `http://link.aps.org/doi/10.1103/PhysRevE.80.026207`

[43] F. T. Arecchi, G. Giacomelli, A. Lapucci, R. Meucci, Two-dimensional representation of a delayed dynamical system, Phys. Rev. A 45 (1992) R4225–R4228. doi:10.1103/PhysRevA.45.R4225.
URL http://link.aps.org/doi/10.1103/PhysRevA.45.R4225

[44] G. Giacomelli, R. Meucci, A. Politi, F. T. Arecchi, Defects and spacelike properties of delayed dynamical systems, Phys. Rev. Lett. 73 (1994) 1099–1102.

[45] G. Giacomelli, A. Politi, Multiple scale analysis of delayed dynamical systems, Physica D 117 (1998) 26–42.

[46] M. Wolfrum, S. Yanchuk, Eckhaus instability in systems with large delay, Phys. Rev. Lett 96 (2006) 220201. doi:10.1103/PhysRevLett.96.220201.

[47] S. Yanchuk, P. Perlikowski, Delay and periodicity, Phys. Rev. E 79 (4) (2009) 046221. doi:10.1103/PhysRevE.79.046221.
URL http://link.aps.org/abstract/PRE/v79/e046221

[48] S. Yanchuk, M. Wolfrum, A multiple time scale approach to the stability of external cavity modes in the Lang-Kobayashi system using the limit of large delay, SIAM J Appl Dyn Syst 9 (2010) 519–535. doi:10.1137/090751335.
URL http://link.aip.org/link/?SJA/9/519/1

[49] S. Yanchuk, L. Lücken, M. Wolfrum, A. Mielke, Spectrum and amplitude equations for scalar delay-differential equations with large delay, Discrete Contin. Dyn. Syst. A 35 (2015) 573.

[50] Stochastics dynamics with delay and memory, Stochastics and Dynamics, 5 (2) [Special Issue] (2005).

[51] F. H. Willeboordse, Time-delayed map phenomenological equivalency with a coupled map lattice, Int. J. of Bifurcation & Chaos 2 (1992) 721. doi:10.1142/S0218127492000847.

[52] I. Fischer, Nichtlineare Dynamik und komplexes raum-zeitliches Verhalten von Halbleiterlasern, Ph.D. thesis, Philipps-Universität Marburg, iSBN: 3922906699,9783922906698 (1995).

[53] J. Javaloyes, T. Ackemann, A. Hurtado, Arrest of domain coarsening via antiperiodic regimes in delay systems, Phys. Rev. Lett. 115 (2015) 203901. doi:10.1103/PhysRevLett.115.203901.
URL http://link.aps.org/doi/10.1103/PhysRevLett.115.203901

[54] X. Porte, O. D'Huys, T. Jüngling, D. Brunner, M. C. Soriano, I. Fischer, Autocorrelation properties of chaotic delay dynamical systems: A study on semiconductor lasers, Phys. Rev. E 90 (2014) 052911.

[55] G. Giacomelli, F. Marin, M. Romanelli, Multi-time-scale dynamics of a laser with polarized optical feedback, Phys. Rev. A 67 (2003) 053809.

[56] S. Lepri, Critical phenomena in delayed maps, Phys. Lett. A 191 (1994) 291–295. doi:10.1016/0375-9601(94)90142-2.

[57] F. T. Arecchi, G. Giacomelli, A. Lapucci, R. Meucci, Dynamics of a CO2 laser with delayed feedback: The short-delay regime, Phys. Rev. A 43 (1991) 4997.

[58] K. Kaneko, Fates of three-torus. i double devil's staircase in lockings, Prog. Theor. Phys. 71 (1984) 282–294. doi:doi: 10.1143/PTP.71.282.

[59] K. Kaneko, Period-doubling of kink-antikink patterns, quasiperiodicity in antiferro-like structures and spatial intermittency in coupled logistic lattice. towards a prelude of a "field theory of chaos", Prog. Theor. Phys. 72 (1984) 480–486. doi:doi: 10.1143/PTP.72.480.

[60] K. Kaneko, Spatiotemporal intermittency in coupled map lattices, Prog. Theor. Phys. 74 (1985) 1033–1044. doi:doi: 10.1143/PTP.74.1033.

[61] S. Yanchuk, M. Wolfrum, Instabilities of equilibria of delay-differential equations with large delay, in: D. van Campen, M. Lazurko, W. van der Oever (Eds.), Proceedings of ENOC-2005, Eindhoven, Netherlands, 2005, pp. 1060–1065.

[62] S. Yanchuk, M. Wolfrum, P. Hövel, E. Schöll, Control of unstable steady states by long delay feedback, Phys. Rev. E 74 (2006) 026201. doi:10.1103/PhysRevE.74.026201.

[63] M. Wolfrum, S. Yanchuk, P. Hövel, E. Schöll, Complex dynamics in delay-differential equations with large delay, Eur. Phys. J. Special Topics 191 (2010) 91–103. doi:10.1140/epjst/e2010-01343-7.
URL http://dx.doi.org/10.1140/epjst/e2010-01343-7

[64] V. Flunkert, S. Yanchuk, T. Dahms, E. Schöll, Synchronizing distant nodes: A universal classification of networks, Phys. Rev. Lett. 105 (25) (2010) 254101. doi:10.1103/PhysRevLett.105.254101.

[65] S. Heiligenthal, T. Dahms, S. Yanchuk, T. Jüngling, V. Flunkert, I. Kanter, E. Schöll, W. Kinzel, Strong and weak chaos in nonlinear networks with time-delayed couplings, Phys. Rev. Lett. 107 (2011) 234102. doi:10.1103/PhysRevLett.107.234102.
URL http://link.aps.org/doi/10.1103/PhysRevLett.107.234102

[66] M. Lichtner, M. Wolfrum, S. Yanchuk, The spectrum of delay differential equations with large delay, SIAM J. Math. Anal. 43 (2011) 788–802. doi:10.1137/090766796.

[67] O. D'Huys, S. Zeeb, T. Jüngling, S. Heiligenthal, S. Yanchuk, W. Kinzel, Synchronisation and scaling properties of chaotic networks with multiple delays, EPL (Europhysics Letters) 103 (1) (2013) 10013.
URL http://stacks.iop.org/0295-5075/103/i=1/a=10013

[68] W. Kinzel, Chaos in networks with time-delayed couplings, Philosophical Transactions of the Royal Society of London A: Mathematical, Physical and Engineering Sciences 371 (2013) 20120461. doi:10.1098/rsta.2012.0461.

[69] S. Heiligenthal, T. Jüngling, O. D'Huys, D. A. Arroyo-Almanza, M. C. Soriano, I. Fischer, I. Kanter, W. Kinzel, Strong and weak chaos in networks of semiconductor lasers with time-delayed couplings, Phys. Rev. E 88 (2013) 012902. doi:10.1103/PhysRevE.88.012902.
URL http://link.aps.org/doi/10.1103/PhysRevE.88.012902

[70] N. Oliver, T. Jüngling, I. Fischer, Consistency properties of a chaotic semiconductor laser driven by optical feedback, Phys. Rev. Lett. 114 (2015) 123902. doi:10.1103/PhysRevLett.114.123902.
URL http://link.aps.org/doi/10.1103/PhysRevLett.114.123902

[71] T. Jüngling, M. C. Soriano, I. Fischer, Determining the sub-lyapunov exponent of delay systems from time series, Phys. Rev. E 91 (2015) 062908. doi:10.1103/PhysRevE.91.062908.
URL http://link.aps.org/doi/10.1103/PhysRevE.91.062908

[72] T. Jüngling, O. D'Huys, W. Kinzel, The transition between strong and weak chaos in delay systems: Stochastic modeling approach, Phys. Rev. E 91 (2015) 062918. doi:10.1103/PhysRevE.91.062918.
URL http://link.aps.org/doi/10.1103/PhysRevE.91.062918

[73] S. R. Dahmen, H. Hinrichsen, W. Kinzel, Space representation of stochastic processes with delay, Phys. Rev. E 77 (2008) 031106. doi:10.1103/PhysRevE.77.031106.
URL http://link.aps.org/doi/10.1103/PhysRevE.77.031106

[74] S. Zeeb, T. Dahms, V. Flunkert, E. Schöll, I. Kanter, W. Kinzel, Discontinuous attractor dimension at the synchronization transition of time-delayed chaotic systems, Phys. Rev. E 87 (2013) 042910. doi:10.1103/PhysRevE.87.042910.
URL http://link.aps.org/doi/10.1103/PhysRevE.87.042910

[75] G. Giacomelli, A. Politi, Relationship between delayed and spatially extended dynamical systems, Phys. Rev. Lett. 76 (15) (1996) 2686–2689.

[76] A. Pikovsky, A. Politi, Lyapunov Exponents: A Tool to Explore Complex Dynamics, Cambridge University Press, 2016.

[77] J. K. Hale, Theory of Functional Differential Equations, Springer-Verlag, 1977.

[78] S. Yanchuk, Properties of stationary states of delay equations with large delay and applications to laser dynamics, Math. Methods Appl. Sci. 28 (2005) 363–377.

[79] M. C. Cross, P. C. Hohenberg, Pattern formation outside of equilibrium, Rev. Mod. Phys. 65 (1993) 851 – 1112.

[80] M. Cross, H. Greenside, Pattern formation and Dynamics in nonequilibrium systems, Cambridge Univ. Press, 2009.

[81] D. Puzyrev, S. Yanchuk, A. Vladimirov, S. Gurevich, Stability of plane wave solutions in complex Ginzburg-Landau equation with delayed feedback, SIAM J. Appl. Dyn. Syst. 13 (2014) 986–1009.

[82] D. Puzyrev, A. Vladimirov, S. Gurevich, S. Yanchuk, Modulational instability and zigzagging of dissipative solitons induced by delayed feedback, Phys. Rev. A, Rapid Communication 93 (032210).

[83] S. Yanchuk, Spectrum in systems with multiple hierarchical time-delays, in preparation.

[84] S. Yanchuk, G. Giacomelli, Dynamical systems with multiple, long delayed feedbacks: Multiscale analysis and spatio-temporal equivalence, Phys. Rev. E 92 (2015) 042903, phys. Rev. E.

[85] S. Yanchuk, G. Giacomelli, Pattern formation in systems with multiple delayed feedbacks, Phys. Rev. Lett. 112 (2014) 174103. doi:10.1103/PhysRevLett.112.174103.
URL `http://link.aps.org/doi/10.1103/PhysRevLett.112.174103`

[86] J. Sieber, M. Wolfrum, M. Lichtner, S. Yanchuk, On the stability of periodic orbits in delay equations with large delay, Discrete Contin. Dyn. Syst. A 33 (2013) 3109–3134.

[87] Y. Pesin, Dimension theory in dynamical systems., Contemporary views and applications. Chicago Lectures in Mathematics., University of Chicago Press, Chicago, IL, 1997.

[88] J. Kaplan, J. Yorke, Functional Differential Equations and Approximation of Fixed Points, Vol. 730, Springer Berlin, 1979, Ch. Chaotic behavior of multidimensional difference equations, pp. 204–227.

[89] S. Yanchuk, J. Sieber, Relative equilibria and relative periodic solutions in systems with time-delay and S^1 symmetry, ArXiv e-prints arXiv:1306.3327 (2003).

[90] Y. Kuznetsov, Elements of Applied Bifurcation Theory, Vol. 112 of Applied Mathematical Sciences, Springer-Verlag, 1995.

[91] H. Chaté, P. Manneville, Phase diagram of the two-dimensional complex ginzburg-landau equation, Physica A: Statistical Mechanics and its Applications 224 (1996) 348 – 368. doi:http://dx.doi.org/10.1016/0378-4371(95)00361-4.
URL `http://www.sciencedirect.com/science/article/pii/0378437195003614`

[92] I. Aranson, L. Kramer, The world of the complex Ginzburg-Landau equation, Rev. Mod. Phys. 74 (2002) 99–143.

[93] R. J. Deissler, K. Kaneko, Velocity-dependent lyapunov exponents as a measure of chaos for open-flow systems, Physics Letters A 119 (8) (1987) 397 – 402. doi:http://dx.doi.org/10.1016/0375-9601(87)90581-0.
URL http://www.sciencedirect.com/science/article/pii/0375960187905810

[94] S. Lepri, A. Politi, A. Torcini, Chronotopic lyapunov analysis. i. a detailed characterization of 1d systems, Journal of Statistical Physics 82 (5-6) (1996) 1429–1452. doi:10.1007/BF02183390.
URL http://dx.doi.org/10.1007/BF02183390

[95] S. Lepri, A. Politi, A. Torcini, Chronotopic lyapunov analysis: Ii. toward a unified approach, Journal of Statistical Physics 88 (1-2) (1997) 31–45. doi:10.1007/BF02508463.
URL http://dx.doi.org/10.1007/BF02508463

[96] R. J. Briggs, Electron-stream interaction with plasmas, MIT Press, Cambridge MA, 1964.

[97] G. Giacomelli, R. Hegger, A. Politi, M. Vassalli, Convective lyapunov exponents and propagation of correlations, Phys. Rev. Lett. 85 (2000) 3616.

[98] R. Hegger, M. J. Bünner, H. Kantz, A. Giaquinta, Identifying and modeling delay feedback systems, Phys. Rev. Lett. 81 (1998) 558.

[99] V. Flunkert, E. Schöll, Pydelay – a python tool for solving delay differential equations, arXiv:0911.1633 [nlin.CD] (2009).

[100] G. Giacomelli, F. Marino, M. A. Zaks, S. Yanchuk, Coarsening in a bistable system with long-delayed feedback, EPL (Europhysics Letters) 99 (2012) 58005.

[101] G. Giacomelli, F. Marino, M. A. Zaks, S. Yanchuk, Nucleation in bistable dynamical systems with long delay, Phys. Rev. E 88 (2013) 062920. doi:10.1103/PhysRevE.88.062920.
URL http://link.aps.org/doi/10.1103/PhysRevE.88.062920

[102] K. Engelborghs, T. Luzyanina, D. Roose, Numerical bifurcation analysis of delay differential equations using dde-biftool, ACM Trans. Math. Software 28 (1) (2002) 1–21. doi:http://doi.acm.org/10.1145/513001.513002.

[103] W. Eckhaus, Studies in Non-Linear Stability Theory, Vol. 6 of Springer Tracts in Natural Philosophy, Springer, New York, 1965.

[104] L. S. Tuckerman, D. Barkley, Bifurcation analysis of the Eckhaus instability, Physica D 46 (1990) 57–86.

[105] S.-N. Chow, J. K. Hale, W. Huang, From sine waves to square waves in delay equations, Proc. Roy. Soc. Edinburgh Sect. A 120 (1992) 223–229.

[106] M. Nizette, Stability of square oscillations in a delayed-feedback system, Phys. Rev. E 70 (2004) 056204.

[107] M. Nizette, Front dynamics in a delayed-feedback system with external forcing, Physica D 183 (2003) 220–244.

[108] L. Weicker, T. Erneux, O. D'Huys, J. Danckaert, M. Jacquot, Y. Chembo, L. Larger, Strongly asymmetric square waves in a time-delayed system, Phys. Rev. E 86 (2012) 055201. doi:10.1103/PhysRevE.86.055201.
URL http://link.aps.org/doi/10.1103/PhysRevE.86.055201

[109] L. Larger, P.-A. Lacourt, S. Poinsot, M. Hanna, From flow to map in an experimental high-dimensional electro-optic nonlinear delay oscillator, Phys. Rev. Lett. 95 (2005) 043903. doi:10.1103/PhysRevLett.95.043903.
URL http://link.aps.org/doi/10.1103/PhysRevLett.95.043903

[110] L. Weicker, T. Erneux, M. Jacquot, Y. Chembo, L. Larger, Crenelated fast oscillatory outputs of a two-delay electro-optic oscillator, Phys. Rev. E 85 (2012) 026206. doi:10.1103/PhysRevE.85.026206.
URL http://link.aps.org/doi/10.1103/PhysRevE.85.026206

[111] G. Dee, W. van Saarloos, Phys. Rev. Lett. 60 (1988) 2641.

[112] A. J. Bray, Theory of phase-ordering kinetics, Adv. Phys. 43 (1994) 357.

[113] L. D. Landau, E. M. Lifshitz, Statistical Physics: Volume 5 (Course of Theoretical Physics), Vol. 5, Elsevier, 1980.

[114] M. Bär, C. Zülicke, M. Eiswirth, G. Ertl, Theoretical modeling of spatiotemporal selforganization in a surface catalyzed reaction exhibiting bistable kinetics, J. Chem. Phys. 96 (1992) 8595.

[115] D. Gomila, P. Colet, G.-L. Oppo, M. S. Miguel, Stable droplets ana nucleation in asymmetric bistable nonlinear optic systems, J. Opt.B: Quantum and Semiclassical Optics 6 (2004) S265–S270.

[116] M. Argentina, P. Coullet, L. Mahadevan, Colliding waves in the model excitable medium: Preservation, annihilation and bifurcation, Phys. Rev. Lett. 79 (1997) 2803.

[117] H. Smith, An Introduction to Delay Differential Equations with Applications to the Life Sciences, Springer New York, 2011.

[118] A. G. Vladimirov, D. Turaev, Model for passive mode locking in semiconductor lasers, Phys. Rev. A 72 (2005) 033808.

[119] M. Nizette, D. Rachinskii, A. Vladimirov, M. Wolfrum, Pulse interaction via gain and loss dynamics in passive mode locking, Physica D 218 (2006) 95–104.

[120] B. Garbin, J. Javaloyes, G. Tissoni, S. Barland, Topological solitons as addressable phase bits in a driven laser, Nat. Commun. 6 (2015) 5915. doi:10.1038/ncomms6915.

[121] M. Marconi, J. Javaloyes, S. Barland, S. Balle, M. Giudici, Vectorial dissipative solitons in vertical-cavity surface-emitting lasers with delays, Nat. Photon. 9 (2015) 450–455. doi:10.1038/nphoton.2015.92.

[122] K. Pyragas, Continuous control of chaos by self-controlling feedback, Physics Letters A 170 (6) (1992) 421–428.
URL http://www.sciencedirect.com/science/article/pii/0375960192907458

[123] T. Hikihara, Y. Ueda, An expansion of system with time delayed feedback control into spatio-temporal state space, Chaos 9 (4) (1999) 887–892. doi:http://dx.doi.org/10.1063/1.166461.
URL http://scitation.aip.org/content/aip/journal/chaos/9/4/10.1063/1.166461

[124] A. L. Franz, R. Roy, L. B. Shaw, I. B. Schwartz, Effect of multiple time delays on intensity fluctuation dynamics in fiber ring lasers, Phys. Rev. E 78 (2008) 016208. doi:10.1103/PhysRevE.78.016208.
URL http://link.aps.org/doi/10.1103/PhysRevE.78.016208

[125] G. Nicolis, I. Prigogine, Self-organization in non equilibrium systems, Wiley, New York, 1977.

[126] F. Marino, G. Giacomelli, S. Barland, Front pinning and localized states analogues in long-delayed bistable systems, Phys. Rev. Lett. 112 (103901) (2014) 103901.

[127] X. Porte, M. C. Soriano, I. Fischer, Similarity properties in the dynamics of delayed-feedback semiconductor lasers, Phys. Rev. A 89 (2014) 023822. doi:10.1103/PhysRevA.89.023822.
URL http://link.aps.org/doi/10.1103/PhysRevA.89.023822

[128] L. Appeltant, M. C. Soriano, G. Van der Sande, J. Danckaert, S. Massar, J. Dambre, B. Schrauwen, C. R. Mirasso, I. Fischer, Information processing using a single dynamical node as complex system, Nature Communications 2 (2011) 468.
URL http://dx.doi.org/10.1038/ncomms1476

[129] L. Larger, M. C. Soriano, D. Brunner, L. Appeltant, J. M. Gutierrez, L. Pesquera, C. R. Mirasso, I. Fischer, Photonic information processing beyond turing: an optoelectronic implementation of reservoir computing, Opt. Express 20 (3) (2012) 3241–3249. doi:10.1364/OE.20.003241.
URL http://www.opticsexpress.org/abstract.cfm?URI=oe-20-3-3241

[130] R. Martinenghi, S. Rybalko, M. Jacquot, Y. K. Chembo, L. Larger, Photonic nonlinear transient computing with multiple-delay wavelength dynamics, Phys. Rev. Lett. 108 (2012) 244101. doi:10.1103/PhysRevLett.108.244101.
URL http://link.aps.org/doi/10.1103/PhysRevLett.108.244101

[131] D. B. Y. Kuramoto, Coexistence of coherence and incoherence in nonlocally coupled phase oscillators, Nonlinear Phenom Complex Syst 5 (2002) 380?385.

[132] L. Larger, B. Penkovsky, Y. Maistrenko, Virtual chimera states for delayed-feedback systems, Phys. Rev. Lett. 111 (2013) 054103. doi:10.1103/PhysRevLett.111.054103.
URL http://link.aps.org/doi/10.1103/PhysRevLett.111.054103

[133] V. Semenov, A. Zakharova, Y. Maistrenko, E. Schöll, Delayed-feedback chimera states: Forced multiclusters and stochastic resonance, EPL (Europhysics Letters) 115 (1) (2016) 10005.
URL http://stacks.iop.org/0295-5075/115/i=1/a=10005

[134] L. Larger, B. Penkovsky, Y. Maistrenko, Laser chimeras as a paradigm for multistable patterns in complex systems, Nat Commun 6 (2015) 7752.
URL http://dx.doi.org/10.1038/ncomms8752

[135] E. G. Turitsyna, S. V. Smirnov, S. Sugavanam, N. Tarasov, X. Shu, S. A. Babin, P. E. V., D. V. Churkin, G. Falkovich, S. K. Turitsyn, The laminar-turbulent transition in a fibre laser, Nat. Photon. 7 (10) (2013) 783–786.
URL http://dx.doi.org/10.1038/nphoton.2013.246

[136] J. K. Jang, M. Erkintalo, S. G. Murdoch, S. Coen, Ultraweak long-range interactions of solitons observed over astronomical distances, Nat Photon 7 (8) (2013) 657–663.
URL http://dx.doi.org/10.1038/nphoton.2013.157

[137] L. A. Lugiato, R. Lefever, Spatial dissipative structures in passive optical systems, Phys. Rev. Lett. 58 (1987) 2209–2211. doi:10.1103/PhysRevLett.58.2209.
URL http://link.aps.org/doi/10.1103/PhysRevLett.58.2209

[138] M. Marconi, J. Javaloyes, S. Balle, M. Giudici, How lasing localized structures evolve out of passive mode locking, Phys. Rev. Lett. 112 (2014) 223901. doi:10.1103/PhysRevLett.112.223901.
URL http://link.aps.org/doi/10.1103/PhysRevLett.112.223901

[139] B. Romeira, R. Avó, J. M. L. Figueiredo, S. Barland, J. Javaloyes, Regenerative memory in time-delayed neuromorphic photonic resonators, Scientific Reports 6 (2016) 19510.
URL http://dx.doi.org/10.1038/srep19510